

Settling accretion onto slowly rotating X-ray pulsars

N. I. Shakura, K. A. Postnov, A. Yu. Kochetkova, L. Hjalmarsdotter

Sternberg Astronomical Institute, Moscow M.V. Lomonosov State University, Universitetskij pr.13, 119992, Moscow, Russia

This work considers a theoretical model for quasi-spherical subsonic accretion onto slowly rotating magnetized neutron stars. In this regime the accreting matter settles down subsonically onto the rotating magnetosphere, forming an extended quasi-static shell. The shell mediates the angular momentum transfer to/from the rotating neutron star magnetosphere by large-scale convective motions, which for observed pulsars lead to an almost so-angular-momentum rotation law with $\omega \sim 1/R^2$ inside the shell. The accretion rate through the shell is determined by the ability of the plasma to enter the magnetosphere due to Rayleigh-Taylor instabilities while taking cooling into account. The settling regime of accretion is possible for moderate accretion rates $\dot{M} \lesssim \dot{M}_* \simeq 4 \times 10^{16}$ g/s. At higher accretion rates a free-fall gap above the neutron star magnetosphere appears due to rapid Compton cooling, and accretion becomes highly non-stationary. From observations of spin-up/spin-down rates of quasi-spherically wind accreting equilibrium X-ray pulsars with known orbital periods (like e.g. GX 301-2 and Vela X-1), it is possible to determine the main dimensionless parameters of the model, as well as to estimate the magnetic field on the surface of the neutron star. For equilibrium pulsars with independent measurements of the magnetic field, the model also allows us to estimate the velocity of the stellar wind from the companion without the use of complicated spectroscopic measurements. For non-equilibrium pulsars, it can be shown that there exists a maximum possible value of the spin-down rate of the accreting neutron star. From observations of the spin-down rate and the X-ray luminosity in such pulsars (e. g. GX 1+4, SXP 1062 and 4U 2206+54) we are able to estimate a lower limit on the neutron star magnetic field, which in all exemplified cases turns out to be close to the standard one and in agreement with cyclotron line measurements. The model further explains both the spin-up/spin-down of the pulsar frequency on large time-scales and the irregular short-term frequency fluctuations, which may correlate or anti-correlate with the X-ray luminosity fluctuations, seen in different systems.

1 Introduction

X-ray pulsars are highly magnetized rotating neutron stars in close binary systems, accreting matter from a companion star. The companion may be a low-mass star overflowing its Roche lobe, in which case an accretion disc is formed. In the case of a high-mass companion, the neutron star may also accrete from the strong stellar wind, and depending on the conditions a disc may be formed or accretion may take place quasi-spherically. The strong magnetic field (of the order of $10^{12} - 10^{13}$ G) of the neutron star disrupts the accretion flow at some distance from the neutron star surface and forces the accreted matter to funnel down on the polar caps of the neutron star creating hot spots that, if misaligned with the rotational axis, make the neutron star pulsate in X-rays. Most accreting pulsars show stochastic variations in their spin frequencies as well as in their luminosities. Many sources also exhibit long-term trends in their spin-behaviour with the period more or less steadily increasing or decreasing, and in some sources spin-reversals have been observed. (For a thorough review, see e.g. [1] and references therein.)

The best-studied case of accretion is that of thin disc accretion [2]. Here the spin-up/spin-down mechanisms are rather well understood. For disc accretion the spin-up torque is determined by the specific angular momentum at the inner edge of the disc and can be written in the form $K_{su} \approx \dot{M} \sqrt{GM R_A}$ [3]. For a pulsar the inner radius of the accretion disc is determined by the Alfvén radius $R_A \sim \dot{M}^{-2/7}$, so $K_{su} \sim \dot{M}^{6/7}$, i.e. for disc accretion the spin-up torque is weakly (almost linearly) dependent on the accretion rate (X-ray luminosity). In contrast, the spin-down torque for disc accretion in the first approximation is independent of \dot{M} : $K_{sd} \sim -\mu^2/R_c^3$, where $R_c = (GM/(\omega^*)^2)^{1/3}$ is the corotation radius, ω^* is the neutron star angular frequency and μ is the neutron star's dipole magnetic moment. In fact, accretion torques in disc accretion are determined by complicated disc-magnetospheric interactions, see, e.g., [4],[5] and the discussion in [6], and correspondingly can have a more complicated dependence on the mass accretion rate and other parameters.

Measurements of spin-up/spin-down in X-ray pulsars can be used to evaluate a very important parameter of the neutron star – its magnetic field. The period of the pulsar is usually close to the equilibrium

value P_{eq} , which is determined by the total zero torque applied to the neutron star, $K = K_{su} + K_{sd} = 0$. So assuming the observed value $\omega^* = 2\pi/P_{eq}$, the magnetic field of the neutron star in disc-accreting X-ray pulsars can be estimated if \dot{M} is known.

In the case of quasi-spherical accretion, which may take place in systems where the optical star underfills its Roche lobe and no accretion disc is formed, the situation is more complicated. Clearly, the amount and sign of the angular momentum supplied to the neutron star from the captured stellar wind are important for spin-up or spin-down. To within a numerical factor of the order of 1 (which can be positive or negative, see numerical simulations by [7],[8], [9], etc.), the torque applied to the neutron star in this case should be proportional to $\dot{M}\omega_B R_B^2$, where $\omega_B = 2\pi/P_B$ is the binary orbital angular frequency, $R_B = 2GM/(V_w^2 + v_{orb}^2)^{1/2}$ is the gravitational capture (Bondi) radius, V_w is the stellar wind velocity at the neutron star orbital distance, and v_{orb} is the neutron star orbital velocity. In real high-mass X-ray binaries the orbital eccentricity is non-zero, the stellar wind is variable and can be inhomogeneous, etc., so K_{su} can be a complicated function of time. The spin-down torque is even more uncertain, since it is impossible to write down a simple equation like $-\mu^2/R_c^3$ any more (R_c has no meaning for quasi-spherical accretion; for slowly rotating pulsars it is much larger than the Alfvén radius where the angular momentum transfer from the accreting matter to the magnetosphere actually occurs). For example, using the expression $-\mu^2/R_c^3$ for the braking torque results in a very high ($\geq 10^{14}$ G) magnetic field for long-period X-ray pulsars. We think this is a result of underestimating the braking torque.

The matter captured from the stellar wind can accrete onto the neutron star in different ways. Indeed, if the X-ray flux from the accreting neutron star is sufficiently high, the shocked matter rapidly cools down due to Compton processes and falls freely toward the magnetosphere. The velocity of motion rapidly becomes supersonic, so a shock is formed above the magnetosphere. This regime was considered, e.g., by [10]. Depending on the sign of the specific angular momentum of falling matter (prograde or retrograde), the neutron star can spin-up or spin-down. However, if the X-ray flux at the Bondi radius is below some value, the shocked matter remains hot, the radial velocity of the plasma is subsonic, and the source may enter the settling accretion regime. A hot quasi-static shell forms around the magnetosphere [11]. Due to additional energy release (especially near the base of the shell), the temperature gradient across the shell becomes superadiabatic, and large-scale convective motions inevitably appear. The convection initiates turbulence, and the motion of a fluid element in the shell becomes quite complicated. If the magnetosphere allows plasma entry via instabilities (and subsequent accretion onto the neutron star), the actual accretion rate through such a shell is controlled by the magnetosphere (for example, a shell can exist, but accretion through it can be weak or even absent altogether). Therefore, on top of the convective motions, the matter acquires a low, on average radial, velocity toward the magnetosphere, and thus subsonic settling is possible. This type of accretion can work only for small X-ray luminosities, $L_x < 4 \times 10^{36}$ erg/s (see below), and is totally different from that considered in the numerical simulations cited above. If a shell is present, its interaction with the rotating magnetosphere can lead to spin-up or spin-down of the neutron star, depending on the sign of the difference of the angular velocity between the accreting matter and the magnetospheric boundary. Thus, in the settling accretion regime, both spin-up or spin-down of the neutron star is possible, even if the sign of the specific angular momentum of the captured matter is always prograde. The shell here mediates the angular momentum transfer to or from the rotating neutron star.

There are several models in the literature (see especially [12] and [13]), from which the expression for the spin-down torque for quasi-spherically accreting neutron stars in the form $K_{sd} \sim -\dot{M}R_A^2\omega^*$ can be derived. Using the standard expression for the Alfvén radius, $R_A \sim \dot{M}^{-2/7}\mu^{4/7}$ this torque is proportional to $K_{sd} \sim -\mu^{8/7}\dot{M}^{3/7}$. In our model, the matter in the shell settles subsonically as the region close to the magnetospheric surface cools down, and the Alfvén radius has a different dependence on the mass accretion rate and the magnetic field, $R_A \sim \dot{M}^{-2/11}\mu^{6/11}$ (see below).

One can show that there are two different mechanisms through which angular momentum can be transferred through a quasi-spherical shell. In the first case (we call this case *moderate coupling*), angular momentum is transferred by convective motions in the shell. The braking torque in the regime of settling accretion with convective removal of angular momentum depends on the accretion rate as $K_{sd} \sim -\dot{M}^{3/11}$ (see Section 4). The velocity of the convective motions in this regime is close to the sound speed. It is also possible to have a settling regime where the angular momentum is removed by shear turbulence in the shell (the *weak coupling regime*). In this regime the characteristic velocities of the shear flow close to the magnetosphere is of the order of the linear rotational velocity. In this case $K_{sd} \sim \mu^2/R_c^3 \sim \mu^2\omega^{*2}/(GM)$, i.e. in the weak coupling regime the torque does not depend on the accretion rate at all.

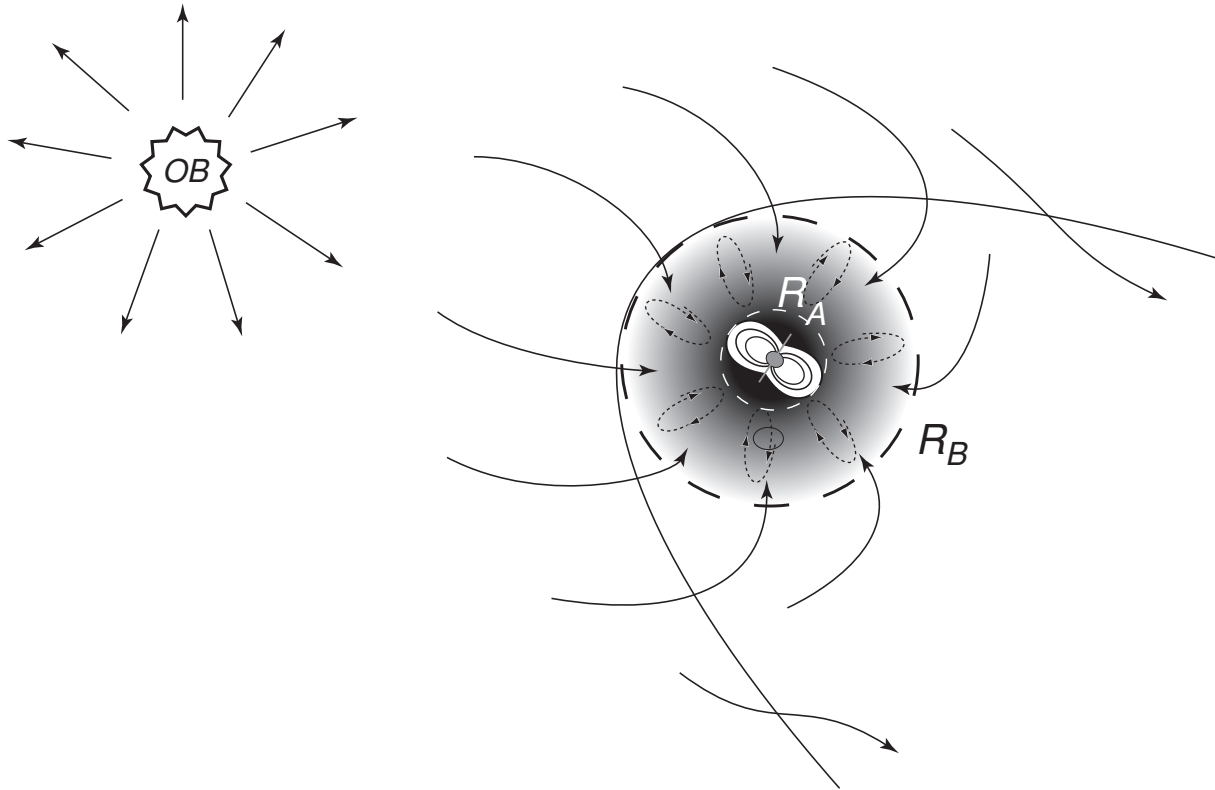


Figure 1: A schematic picture of quasi-spherical accretion from the stellar wind of an optical companion star (left) onto a neutron star (right) in a binary system. In the regime of subsonic accretion, a quasi-spherical shell (shaded area) of radius R_A is formed between the bow shock (parabolic curve) and the rotating magnetosphere. In this shell, large-scale convective motions are formed that may act to remove angular momentum from the magnetosphere. The outer radius of the shell is determined by the gravitational capture or Bondi radius R_B . The characteristic velocity of the wind is $v_w \sim 300 - 1000$ km/s. The contour arrow shows the direction of the orbital velocity of the neutron star v_{orb} .

To stress the difference between the two possible regimes of subsonic accretion (with moderate and weak coupling), we can rewrite the expression for the braking torque with convection (moderate coupling) using the corotational radius and the Alfvén radius in the form $K_{sd} \sim -\mu^2/\sqrt{R_c^3 R_A^3} \sim -(\mu^2/R_c^3)(R_c/R_A)^{3/2}$ (see further details in Section 3). Since the factor $(R_c/R_A)^{3/2} \sim (\omega_K(R_A)/\omega^*)$ can be of the order of 10 or more in real systems, using a braking torque in the form of μ^2/R_c^3 may lead to a strong overestimate of the magnetic field of the neutron star.

The dependence of the braking torque on the accretion rate in the case of quasi-spherical settling accretion suggests that variations of the mass accretion rate (and X-ray luminosity) must lead to a transition from spin-up (at high accretion rates) to spin-down (at small accretion rates) at some critical value of \dot{M} (or R_A), that differs from source to source. This phenomenon (known as torque reversal) is actually observed in wind-fed pulsars like Vela X-1, GX 301-2 and GX 1+4, which we shall consider below in more detail.

The structure of this paper is as follows. In Section 2, we present an outline of the theory for quasi-spherical accretion onto a neutron star magnetosphere. We show that it is possible to construct a hot envelope around the neutron star through which subsonic accretion can take place and act to either spin up or spin down the neutron star. In Section 3, we discuss the structure of the interchange instability region which determines whether the plasma can enter the magnetosphere of the rotating neutron star. In Section 4 we consider how the spin-up/spin-down torques vary with a changing accretion rate. In Section 5, we show how to determine the parameters of quasi-spherical accretion from observational data. In Section 6, we apply our methods to the specific pulsars GX 301-2, Vela X-1, GX 1+4, SXP 1062 and 4U 2206+54. In Section 7 we discuss our results and, finally, in Section 8 we present our conclusions. A detailed gas-dynamic treatment of the problem is presented in five appendices, which are very important to understand the physical processes involved.

This work follows to a large extent the earlier published paper of [14]. However, here are included several additions, clarifying and refining the physical model (especially in Sections 1-4 and in Conclusions.

2 Quasi-spherical accretion

2.1 The structure of a subsonic shell around a neutron star magnetosphere

We shall here consider the torques applied to a neutron star in the case of quasi-spherical accretion from a stellar wind. Wind matter is gravitationally captured by the moving neutron star and a bow-shock is formed at a characteristic distance $R \sim R_B$, where R_B is the Bondi radius. Angular momentum can be removed from the neutron star magnetosphere in two ways — either with matter expelled from the magnetospheric boundary without accretion (the propeller regime, [15]), or via large-scale convective motions in a subsonic quasi-static shell around the magnetosphere, in which case the accretion rate onto the neutron star is determined by the ability of the plasma to enter the magnetosphere, in the regime of subsonic accretion.

In such a quasi-static shell, the temperature will be high (of the order of the virial temperature, see [11]), and the important point is whether hot matter from the shell can in fact enter the magnetosphere. Two-dimensional calculations by [16] have shown that hot monoatomic ideal plasma is stable relative to the Rayleigh-Taylor instability at the magnetospheric boundary, and plasma cooling is thus needed for accretion to begin. However, a closer inspection of the 3-dimensional calculations by [17] reveals that the hot plasma is only marginally stable at the magnetospheric equator (to within 5% accuracy of their calculations). Compton cooling and the possible presence of dissipative phenomena (magnetic reconnection etc.) facilitates the plasma entering the magnetosphere. We will show below that spin-down of the neutron star is possible in the case of accretion of matter from a hot envelope in the subsonic settling regime.

To a zeroth approximation, we can neglect both rotation and radial motion (accretion) of matter in the shell and consider only its equilibrium hydrostatic structure. The radial velocity of matter falling through the shell u_R is lower than the sound velocity c_s . Under these assumptions, the characteristic cooling/heating time-scale is much larger than the free-fall time-scale.

In the general case where both gas pressure and anisotropic turbulent motions are present, Pascal's law is violated. Then the hydrostatic equilibrium equation can be derived from the equation of motion

(A.16) with stress tensor components (A.19) - (A.21) and zero viscosity (see Appendix A for more detail):

$$-\frac{1}{\rho} \frac{dP_g}{dR} - \frac{1}{\rho R^2} \frac{d(P_{\parallel}^t R^2)}{dR} + \frac{2P_{\perp}^t}{\rho R} - \frac{GM}{R^2} = 0 \quad (1)$$

Here $P_g = \rho c_s^2 / \gamma$ is the gas pressure, and P^t stands for the pressure due to turbulent motions:

$$P_{\parallel}^t = \rho \langle u_{\parallel}^2 \rangle = \rho m_{\parallel}^2 c_s^2 = \gamma P_g m_{\parallel}^2 \quad (2)$$

$$P_{\perp}^t = \rho \langle u_{\perp}^2 \rangle = \rho m_{\perp}^2 c_s^2 = \gamma P_g m_{\perp}^2 \quad (3)$$

($\langle u_t^2 \rangle = \langle u_{\parallel}^2 \rangle + 2 \langle u_{\perp}^2 \rangle$ is the turbulent velocity dispersion, m_{\parallel}^2 and m_{\perp}^2 are turbulent Mach numbers squared in the radial and tangential directions, respectively; for example, in the case of isotropic turbulence $m_{\parallel}^2 = m_{\perp}^2 = (1/3)m_t^2$ where m_t is the turbulent Mach number). The total pressure is the sum of the gas and turbulence terms: $P_g + P_t = P_g(1 + \gamma m_t^2)$.

The turbulent Mach number in the shell may in general depend on the radius. In our case, however, we will consider it constant. Furthermore, in real pulsars, turbulent heating (important from a dynamic point of view, see Appendix E) will change the estimated parameters by less than a factor of 2 (see formulas in Section 6).

We shall consider, to a first approximation, that the entropy S is constant throughout the shell. For an ideal gas with adiabatic index γ and equation of state $P = K e^{S/cv} \rho^{\gamma}$, the density can be expressed as a function of temperature: $\rho \sim T^{1/(\gamma-1)}$. Integrating the hydrostatic equilibrium equation (1), we find:

$$\frac{RT}{\mu_m} = \left(\frac{\gamma-1}{\gamma} \right) \frac{GM}{R} \left(\frac{1}{1 + \gamma m_{\parallel}^2 - 2(\gamma-1)(m_{\parallel}^2 - m_{\perp}^2)} \right) = \frac{\gamma-1}{\gamma} \frac{GM}{R} \psi(\gamma, m_t). \quad (4)$$

(In this solution we have neglected the integration constant, which is not important deep inside the shell. It is important in the outer part of the shell, but since the outer region close to the bow shock at $\sim R_B$ is not spherically symmetric, its structure can only be found numerically). We note that taking turbulence into account somewhat decreases the temperature within the shell. Most important, however, is that the anisotropy of turbulent motions, caused by convection, in the stationary case changes the distribution of angular velocity in the shell. Below we will show that in the case of isotropic turbulence, the angular velocity distribution within the shell is close to quasi-Keplerian: $\omega(R) \sim R^{-3/2}$. In the case of strongly anisotropic turbulence caused by convection, $m_{\parallel}^2 \gg m_{\perp}^2$, the distribution of momentum in the shell may become almost iso-angular: $\omega(R) \sim R^{-2}$. Below we shall see that an analysis of several real X-ray pulsars favors an iso-angular momentum rotation distribution.

Now, let us write down how the density varies inside the quasi-static shell for $R \ll R_B$. For a fully ionized gas with $\gamma = 5/3$ we find:

$$\rho(R) = \rho(R_A) \left(\frac{R_A}{R} \right)^{3/2} \quad (5)$$

$$P(R) = P(R_A) \left(\frac{R_A}{R} \right)^{5/2}. \quad (6)$$

The above equations describe the structure of an ideal static adiabatic shell above the magnetosphere. Of course, at $R \sim R_B$ the problem is essentially non-spherically symmetric and numerical simulations are required.

Corrections to the adiabatic temperature gradient due to convective energy transport through the shell are calculated in Appendix D.

2.2 The Alfvén surface

At the magnetospheric boundary (the Alfvén surface), the total pressure (including isotropic gas pressure and the possibly anisotropic turbulent pressure) is balanced by the magnetic pressure $B^2/(8\pi)$

$$P_g + P_t = P_g(R_A)(1 + \gamma m_t^2) = \frac{B^2(R_A)}{8\pi}. \quad (7)$$

The magnetic field at the Alfvén radius is determined by the dipole moment and magnetic field of the neutron star and by electric currents flowing on the Alfvénic surface (in the magnetopause):

$$P_g(R_A) = \frac{K_2}{(1 + \gamma m_t^2)} \frac{B_0^2}{8\pi} \left(\frac{R_0}{R_A} \right)^6 = \frac{\rho \mathcal{R} T}{\mu_m} \quad (8)$$

where the dimensionless coefficient K_2 takes into account the contribution from these currents and the factor $1/(1 + \gamma m_t^2)$ is due to the turbulent pressure term. For example, in the model by Arons and Lea [17] (their Eq. 31), $K_2 = (2.75)^2 \approx 7.56$. At the magnetospheric cusp (where the magnetic force line is branched), the radius of the Alfvén surface is about 0.51 times that of the equatorial radius [17]. Below we shall assume that R_A is the equatorial radius of the magnetosphere, unless stated otherwise.

The plasma is able to enter the magnetosphere mainly due to the interchange instability. In the stationary regime, let us introduce the accretion rate \dot{M} onto the neutron star surface. From the continuity equation in the shell we find

$$\rho(R_A) = \frac{\dot{M}}{4\pi u_R(R_A) R_A^2} \quad (9)$$

Clearly, the velocity of absorption of matter by the magnetosphere is smaller than the free-fall velocity, so we introduce a dimensionless factor $f(u) = u_R/\sqrt{2GM/R} < 1$. Then the density at the magnetospheric boundary is

$$\rho(R_A) = \frac{\dot{M}}{4\pi f(u) \sqrt{2GM/R_A} R_A^2}. \quad (10)$$

For example, in the model calculations by [17], $f(u) \approx 0.1$; in our case, at high X-ray luminosities, the value of $f(u)$ may attain ≈ 0.5 . If we imagine that the shell is impenetrable and that there is no accretion through it, $\dot{M} \rightarrow 0$. In this case $u_R \rightarrow 0$, $f(u) \rightarrow 0$, while the density in the shell remains finite. In some sense, the matter is leaking from the magnetosphere down onto the neutron star, and the leakage may be either very small ($\dot{M} \rightarrow 0$) or have a finite non-zero value ($\dot{M} \neq 0$).

Plugging $\rho(R)$ into (8) and using (4) and the definition of the dipole magnetic moment

$$\mu = \frac{1}{2} B_0 R_0^3$$

(where R_0 is the neutron star radius), we find an expression for the Alfvén radius in the case of quasi-spherical accretion:

$$R_A = \left[\frac{4\gamma}{(\gamma - 1)} \frac{f(u) K_2}{\psi(\gamma, m_t) (1 + \gamma m_t^2)} \frac{\mu^2}{\dot{M} \sqrt{2GM}} \right]^{2/7}. \quad (11)$$

It should be stressed that in the presence of a hot shell the Alfvén radius is determined by the static gas pressure (with a possible addition of turbulent motions) at the magnetospheric boundary, which is non-zero even for a zero-mass accretion rate through the shell. The dependence of $f(u)$ on the accretion rate \dot{M} in the case of a settling shell taking cooling into account will be derived below (see (33) below). In the supersonic (Bondi) regime we obviously have $f(u) = 1$. We note that accretion with subsonic velocity can take place even in the Bondi regime, but with significantly lower accretion rate (as compared to the maximum). In the Bondi regime (i.e. in the adiabatic regime without gas heating and/or cooling), the choice of solution depends on the boundary conditions.

2.3 The mean velocity of matter entering through the magnetospheric boundary

As mentioned above, the plasma enters the magnetosphere of the slowly rotating neutron star due to the interchange instability. The boundary between the plasma and the magnetosphere is stable at high temperatures $T > T_{cr}$, but becomes unstable at $T < T_{cr}$, and remains in a neutral equilibrium at $T = T_{cr}$ [16]. The critical temperature is:

$$\mathcal{R} T_{cr} = \frac{1}{2(1 + \gamma m_t^2)} \frac{\cos \chi}{\kappa R_A} \frac{\mu_m GM}{R_A}. \quad (12)$$

Here κ is the local curvature of the magnetosphere, χ is the angle the outer normal makes with the radius-vector at a given point, and the contribution of turbulent pulsations in the plasma to the total

pressure is taken into account by the factor $(1 + \gamma m_t^2)$. The effective gravity acceleration can be written as

$$g_{eff} = \frac{GM}{R_A^2} \cos \chi \left(1 - \frac{T}{T_{cr}} \right). \quad (13)$$

The temperature in the quasi-static shell is given by (4), and the condition for the magnetosphere instability can thus be rewritten as:

$$\frac{T}{T_{cr}} = \frac{2(\gamma - 1)(1 + \gamma m_t^2)}{\gamma} \psi(\gamma, m_t) \frac{\kappa R_A}{\cos \chi} < 1. \quad (14)$$

According to [17], when the external gas pressure decreases with radius as $P \sim R^{-5/2}$, the form of the magnetosphere far from the polar cusp can be described to within 10% accuracy as $(\cos \lambda)^{0.2693}$ (here λ is the polar angle counting from the magnetospheric equator). The instability first appears near the equator, where the curvature is minimal. Near the equatorial plane ($\lambda = 0$), for a poloidal dependence of the magnetosphere $\approx (\cos \lambda)^{0.27}$ we get for the curvature $k_p R_A = 1 + 0.27$. The toroidal field curvature at the magnetospheric equator is $k_t = 1$. The tangent sphere at the equator cannot have a radius larger than the inverse poloidal curvature, therefrom $\kappa R_A = 1.27$ at $\lambda = 0$. This is somewhat larger than the value of $\kappa R_A = \gamma/(2(\gamma - 1)) = 5/4 = 1.25$ (for $\gamma = 5/3$ in the absence of turbulence or for fully isotropic turbulence), but within the accuracy limit¹. The contribution from anisotropic turbulence decreases the critical temperature; for example, for $\gamma = 5/3$, in the case of strongly anisotropic turbulence $m_{\parallel} = 1$, $m_{\perp} = 0$, at $\lambda = 0$ we obtain $T/T_{cr} \sim 2$, i.e. anisotropic turbulence increases the stability of the magnetosphere. So initially the plasma-magnetospheric boundary is stable, and after cooling to $T < T_{cr}$ the plasma instability sets in, starting in the equatorial zone, where the curvature of the magnetospheric surface is minimal.

Let us consider the development of the interchange instability when cooling (predominantly Compton cooling) is present. The temperature changes as [19], [20]

$$\frac{dT}{dt} = -\frac{T - T_x}{t_C}, \quad (15)$$

$$t_C = \frac{3}{2\mu_m} \frac{\pi R_A^2 m_e c^2}{\sigma_T L_x} \approx 10.6 [\text{s}] R_9^2 \dot{M}_{16}^{-1}. \quad (16)$$

where the Compton cooling time is

$$t_C = \frac{3}{2\mu_m} \frac{\pi R_A^2 m_e c^2}{\sigma_T L_x} \approx 10.6 [\text{s}] R_9^2 \dot{M}_{16}^{-1}. \quad (17)$$

Here m_e is the electron mass, σ_T is the Thomson cross section, $L_x = 0.1 \dot{M} c^2$ is the X-ray luminosity, T is the electron temperature (which is equal to the ion temperature since the timescale of electron-ion energy exchange here is the shortest possible), T_x is the X-ray temperature and $\mu_m = 0.6$ is the molecular weight. The photon temperature is $T_x = (1/4)T_{cut}$ for a bremsstrahlung spectrum with an exponential cut-off at T_{cut} , typically $T_x = 3 - 5$ keV. The solution of equation (15) reads:

$$T = T_x + (T_{cr} - T_x) e^{-t/t_C}. \quad (18)$$

We note that $T_{cr} \sim 30$ keV $\gg T_x \sim 3$ keV. It is seen that for $t \approx 2t_C$ the temperature decreases to T_x . In the linear approximation the temperature changes as:

$$T \approx T_{cr}(1 - t/t_C). \quad (19)$$

Plugging this expression into (13), we find that the effective gravity acceleration increases linearly with time as:

$$g_{eff} \approx \frac{GM}{R_A^2} \frac{t}{t_C} \cos \chi. \quad (20)$$

Correspondingly, the velocity of matter due to the instability growth increases with time as:

$$u_r = \int_0^{t_{inst}} g_{eff} dt = \frac{GM}{R_A^2} \frac{t_{inst}^2}{2t_C} \cos \chi. \quad (21)$$

¹In [30], the curvature is calculated to be $\kappa R_A \approx 1.34$, still within the accuracy limit

Here, t_{inst} is the characteristic time of the instability which can be expressed in the form:

$$t_{inst} = \frac{K_0}{\omega_K(R_A)} \frac{u_{ff}}{u_r} = \frac{K_0}{\omega_K(R_A)f(u)}. \quad (22)$$

The choice of this expression is due to the fact that in the case of rapid cooling, the velocity of matter u_r is of the order of the free-fall time u_{ff} , and for slow cooling $u_r \ll u_{ff}$. We have also defined $f(u) \equiv u_r/u_{ff} < 1$, which will be used in the following. K_0 is a dimensionless constant of the order of unity.

Plugging t_{inst} into (21), we find the velocity obtained by the matter during the time-scale of the instability:

$$u_r(t_{inst}) = \frac{K_0^2}{2} \frac{R_A}{t_C f(u)^2} \cos \chi. \quad (23)$$

Dividing both parts of this equation by u_{ff} and solving for $f(u)$, we get the expression for $f(u)$:

$$f(u) = \left(\frac{K_0^2}{2}\right)^{1/3} \left(\frac{t_{ff}}{t_C}\right)^{1/3} (\cos \chi)^{1/3}. \quad (24)$$

We used here the expression for the free-fall time:

$$t_{ff} \equiv \frac{R_A}{u_{ff}(R_A)} = \frac{R_A^{3/2}}{\sqrt{2GM}}. \quad (25)$$

Then, the characteristic time-scale for the instability can be rewritten in the form:

$$t_{inst} = \frac{(2K_0)^{1/3}}{\omega_K(R_A)} \left(\frac{t_C}{t_{ff}}\right)^{1/3} (\cos \chi)^{-1/3}. \quad (26)$$

From this it can be seen that for $t_C \gg t_{ff}$, the timescale for the instability is much larger than the free-fall time.

$$\frac{t_{inst}}{t_{ff}} = 2^{1/2} (2K_0)^{1/3} \left(\frac{t_C}{t_{ff}}\right)^{1/3} (\cos \chi)^{-1/3} \quad (27)$$

On the other hand, the time-scale of the instability is shorter than the Compton cooling time:

$$\frac{t_{inst}}{t_C} = 2^{1/2} (2K_0)^{1/3} \left(\frac{t_{ff}}{t_C}\right)^{2/3} (\cos \chi)^{-1/3} < 1, \quad (28)$$

which allows us to use the linear expansion of temperature increase as a function of time time (19).

The characteristic scale of instability growth is:

$$\Delta = \int_0^{t_{inst}} u_r dt = \frac{1}{6} \frac{GM}{R_A^2} \frac{t_{inst}^3}{t_C} \cos \chi = \frac{1}{3} u_r t_{inst} = \frac{\sqrt{2}}{3} K_0 R_A. \quad (29)$$

In this way, during t_{inst} , the scale of the instability becomes comparable to the magnetospheric radius, and the settling velocity turns out to be much smaller than free-fall velocity u_{ff} . Clearly, later in the non-linear stage of the instability growth the velocity of matter approaches the free-fall velocity. We mainly consider the linear stage, since at this stage the temperature is still high enough (although the entropy starts decreasing with decreasing radius), and it is in this zone that a toroidal component of the magnetic field is formed and effective angular momentum transfer from the magnetosphere to the shell can take place. At later stages of instability growth, the loss of entropy is too strong for convection to begin.

Let us estimate the accuracy of our approximation by retaining the second-order terms in the exponent expansion. Then the velocity the matter acquires during the instability time t_{inst} is:

$$u_r(t_{inst}) = K_0^{2/3} \left(\frac{GM}{t_C}\right)^{1/3} (\cos \chi)^{1/3} \left[1 - \frac{2^{5/6} K_0^{1/3}}{3} \left(\frac{t_{ff}}{t_C}\right)^{2/3} (\cos \chi)^{-1/3}\right]. \quad (30)$$

Clearly, the smaller accretion rate, the smaller the ratio t_{ff}/t_C , and the better our approximation.

We note that for the magnetospheric radius in the form $\sim \cos \lambda^n$ we have $\tan \chi = n \tan \lambda$. Therefore, for $n \simeq 0.27$ close to the equator $\cos \chi \simeq 1$ with high accuracy, and we will in the following ignore this factor. We also note that in the magnetospheric cusp region $\cos \chi \simeq 0$, and in this region matter can almost not enter the magnetosphere at all. Substituting (17) into (24) and then $f(u)$ into definition (11), we find for $\gamma = 5/3$ the expression for the Alfvén radius in this regime:

$$R_A \approx 1.55 \times 10^9 [\text{cm}] K_0^{2/11} \left[\left(1 + \frac{5}{3} m_t^2 \right) \psi \left(\frac{5}{3}, m_t \right) \right]^{-3/11} \left(\frac{\mu_{30}^3}{M_{16}} \right)^{2/11}. \quad (31)$$

We stress the difference of the obtained expression for the Alfvén radius with the standard one, $R_A \sim \mu^{4/7}/\dot{M}^{-2/7}$, which is obtained by equating the dynamical pressure of falling gas to the magnetic field pressure; this difference comes from the dependence of $f(u)$ on the magnetic moment and mass accretion rate in the settling accretion regime.

The coefficient due to turbulence

$$K_t = \left(1 + \frac{5}{3} m_t^2 \right) \psi \left(\frac{5}{3}, m_t \right) \quad (32)$$

is obviously equal to 1 for isotropic turbulence (see the expression for ψ (4)), and thus of interest only in the case of anisotropic turbulence.

Plugging (31) into (24), we obtain an explicit expression for $f(u)$:

$$f(u) \approx 0.39 K_0^{7/11} K_t^{1/22} \dot{M}_{16}^{4/11} \mu_{30}^{-1/11}. \quad (33)$$

A necessary condition for removal of angular momentum from the magnetosphere via convection is the condition of subsonic settling (the Mach number for the settling velocity $\mathcal{M} \equiv u_r/c_s < 1$), which for $\gamma = 5/3$ is reduced to the inequality $f(u) < 1/\sqrt{3}$. Clearly, this condition is fulfilled for mass accretion rates around 10^{16} g/s and lower. It is also important to stress that convection in the shell as well as removal of angular momentum practically stops working when the mean radial settling velocity of the matter u_r becomes higher than the convective velocity u_c , i.e. when the convective Mach number $m_c = u_c/c_s \sim m_t$ becomes smaller than the standard Mach number $\mathcal{M} = u_r/c_s$. And oppositely, when the Mach number of the radial flow becomes smaller than the turbulent Mach number $\mathcal{M} < m_t \sim m_c$, removal of angular momentum through the shell may take place. When the accretion rate of matter through the shell becomes larger than a certain critical value $\dot{M} > \dot{M}^\dagger$ the velocity of the accretion flow close to the Alfvénic surface may become higher than the sound speed, and a supersonic flow region with matter in free fall may form above the magnetosphere. Through this region it is not possible to remove any angular momentum from the rotating magnetosphere. In this case, settling accretion is not applicable. A shockwave forms above the magnetosphere and plasma interaction with the magnetosphere is described in the scenario studied in e.g. [10]. Depending on the inhomogeneity of the captured stellar wind, the specific angular momentum may be either positive or negative, and thus alternating episodes of spin-up and spin-down of the neutron star are possible in the supersonic regime. It is easy to estimate the critical X-ray luminosity above which the transition from the subsonic (at low X-ray luminosities) to the Bondi-Hoyle-Littleton (at high X-ray luminosities) regime takes place. Indeed, assuming a limit for the dimensionless settling velocity of $f(u)=0.5$ (at which removal of angular momentum through the shell is still possible, see further Appendix E), from equation (33), we find the maximum possible value of the accretion rate for the settling regime with removal of angular momentum:

$$\dot{M}_{16}^\dagger \approx 2 K_0^{-7/4} K_t^{-1/8} \mu_{30}^{1/4}. \quad (34)$$

We note that a similar value for the critical accretion rate can be found from a comparison of the Compton cooling time to the time-scale for convection close to the Alfvén radius.

To conclude this section, we note that it is not difficult to perform a similar analysis for the velocity of matter in the magnetosphere due to radiative cooling of the plasma, for cases when Compton cooling is less effective [21]. This scenario may be realized in X-ray pulsars at very low accretion rates when the shape of the X-ray beam-pattern changes and the photon beam forms a pencil diagram illuminating the magnetospheric cusp. In this way one can explain the episodic off-states (with very low X-ray luminosity), accompanied with a phase-shift in the X-ray pulse profile [22] as observed in pulsars like e.g. Vela X-1.

3 Transfer of angular momentum to the magnetosphere

Let us now consider a quasi-stationary subsonic shell in which accretion proceeds onto the neutron star magnetosphere. We stress that in this regime, i.e. the settling regime, the accretion rate onto the neutron star is determined by the density at the bottom of the shell (which is directly related to the density downstream the bow shock in the gravitational capture region) and the ability of the plasma to enter the magnetosphere through the Alfvénic surface.

The rotation law in the shell depends on the treatment of the turbulent viscosity (see Appendix B for cases when the Prandtl law and isotropic turbulence are applicable) and the possible anisotropy of the turbulence due to convection (see Appendix C). In the latter case the anisotropy leads to more powerful radial turbulence than perpendicular. In this way, as shown in Appendix B and C, we arrive at a set of quasi-power-law solutions for the radial dependence of the angular rotation velocity in a convective shell. We shall in the following consider a simple power-law dependence of the angular momentum on radius,

$$\omega(R) \sim R^{-n}. \quad (35)$$

In Section 5 in applications to real pulsars we will use a quasi-Keplerian law with $n = 3/2$ as well as an iso-angular momentum distribution with $n = 2$, which in some sense represent limiting cases among possible solutions.

When approaching the bow shock, $R \rightarrow R_B$, and the angular velocity of matter approaches the orbital velocity, $\omega \rightarrow \omega_B$. Close to the bow shock the problem is not spherically symmetric any more since the flow becomes very complex (parts of the flow may cause the hot shell to bend, etc.), and the structure of the flow can be studied only using numerical simulations. In the absence of such simulations, we shall assume that the assumption of an iso-angular momentum distribution is valid up to the front of the bow shock located at a distance from the neutron star which we shall take to be the Bondi radius R_B ,

$$R_B \simeq 2GM/(V_w^2 + v_{orb}^2)^2$$

where V_w is the stellar wind velocity at the neutron star orbital distance, and v_{orb} is the neutron star orbital velocity.

This means that the angular velocity of rotation of matter near the magnetosphere ω_m will be related to ω_B via

$$\omega_m = \tilde{\omega} \omega_B \left(\frac{R_B}{R_A} \right)^n. \quad (36)$$

(Here the numerical factor $\tilde{\omega} > 1$ takes into account the deviation of the actual rotational law from the value obtained by using the assumed power-law dependence near the Alfvén radius; see Appendix B and C for more detail.)

Now, let the NS magnetosphere rotate with an angular velocity $\omega^* = 2\pi/P^*$ where P^* is the neutron star spin period. The matter at the bottom of the shell rotates with an angular velocity ω_m , in general different from ω^* . If $\omega^* > \omega_m$, coupling of the plasma with the magnetosphere ensures transfer of angular momentum from the magnetosphere to the shell, or from the shell to the magnetosphere if $\omega^* < \omega_m$. In the general case, the coupling of matter with the magnetosphere can be moderate or strong. In the strong coupling regime the toroidal magnetic field component B_t is proportional to the poloidal field component B_p as $B_t \sim -B_p(\omega_m - \omega^*)t$, and $|B_t|$ can grow to $\sim |B_p|$. This regime can be expected for rapidly rotating magnetospheres when ω^* is comparable to or even greater than the Keplerian angular frequency $\omega_K(R_A)$; in the latter case the propeller regime sets in. In the moderate coupling regime, the plasma can enter the magnetosphere due to instabilities on a timescale shorter than the time needed for the toroidal field to grow to the value of the poloidal field, so $B_t < B_p$.

3.1 The case of strong coupling

Let us first consider the strong coupling regime. In this regime, powerful large-scale convective motions may lead to turbulent magnetic field diffusion accompanied by magnetic field dissipation. This process is characterized by the turbulent magnetic field diffusion coefficient η_t . In this case the toroidal magnetic field (see e.g. [5] and references therein) is:

$$B_t = \frac{R^2}{\eta_t} (\omega_m - \omega^*) B_p. \quad (37)$$

The turbulent magnetic diffusion coefficient is related to the kinematic turbulent viscosity as $\eta_t \simeq \nu_t$. The latter can be written as:

$$\nu_t = \langle u_t l_t \rangle. \quad (38)$$

According to the phenomenological Prandtl law, the average characteristics of a turbulent flow (the velocity u_t , the characteristic scale of turbulence l_t and the shear $\omega_m - \omega^*$) are related as:

$$u_t \simeq l_t |\omega_m - \omega^*|. \quad (39)$$

In our case, the turbulent scale must be determined by the largest scale of energy supply to the turbulence from the rotation of the non-spherical magnetospheric surface. This scale is determined by the difference in velocity between the solidly rotating magnetosphere and the accreting matter that is still not interacting with the magnetosphere, i.e. $l_t \simeq R_A$, which determines the turn-over velocity of the largest turbulence eddies. At smaller scales a turbulent cascade develops. Substituting this scale into equations (37)-(39) above, we find that in the strong coupling regime $B_t \simeq B_p$.

The momentum of the forces due to plasma-magnetosphere interactions acts on the neutron star and changes its spin according to:

$$I\dot{\omega}^* = \int \frac{B_t B_p}{4\pi} \varpi dS = \pm \tilde{K}(\theta) K_2 \frac{\mu^2}{R_A^3} \quad (40)$$

where I is the neutron star's moment of inertia, ϖ is the distance from the rotational axis and $\tilde{K}(\theta)$ is a numerical coefficient depending on the angle between the rotational and magnetic dipole axes. The coefficient K_2 appears in the above expression for the same reason as in (8). The positive sign corresponds to positive flux of angular momentum to the neutron star ($\omega_m > \omega^*$). The negative sign corresponds to negative flux of angular momentum across the magnetosphere ($\omega_m < \omega^*$).

At the Alfvén radius, the matter couples with the magnetosphere and acquires the angular velocity of the neutron star. It then falls onto the neutron star surface and returns the angular momentum acquired at R_A back to the neutron star via the magnetic field. As a result of this process, the neutron star spins up at a rate determined by the expression:

$$I\dot{\omega}^* = +z\dot{M}R_A^2\omega^* \quad (41)$$

where z is a numerical coefficient which takes into account the angular momentum of the falling matter. If all matter falls from the equatorial equator, $z = 1$; if matter falls strictly along the spin axis, $z = 0$. If all matter were to fall across the entire magnetospheric surface, then $z = 2/3$.

Ultimately, the total torque applied to the neutron star in the strong coupling regime yields

$$I\dot{\omega}^* = \pm \tilde{K}(\theta) K_2 \frac{\mu^2}{R_A^3} + z\dot{M}R_A^2\omega^*. \quad (42)$$

Using (11), we can eliminate \dot{M} in the above equation to obtain in the spin-up regime ($\omega_m > \omega^*$)

$$I\dot{\omega}^* = \frac{\tilde{K}(\theta)K_2\mu^2}{R_A^3} \left[1 + z \frac{4\gamma f(u)}{\sqrt{2}(\gamma-1)(1+\gamma m_t^2)\psi(\gamma, m_t)\tilde{K}(\theta)} \left(\frac{R_A}{R_c} \right)^{3/2} \right] \quad (43)$$

where $R_c^3 = GM/(\omega^*)^2$ is the corotation radius. In the spin-down regime ($\omega_m < \omega^*$) we find

$$I\dot{\omega}^* = -\frac{\tilde{K}(\theta)K_2\mu^2}{R_A^3} \left[1 - z \frac{4\gamma f(u)}{\sqrt{2}(\gamma-1)(1+\gamma m_t^2)\psi(\gamma, m_t)\tilde{K}(\theta)} \left(\frac{R_A}{R_c} \right)^{3/2} \right]. \quad (44)$$

Note that in both cases R_A must be smaller than R_c , otherwise the propeller effect prohibits accretion. In the propeller regime $R_A > R_c$, matter does not fall onto the neutron star, there are no accretion-generated X-rays from the neutron star, the shell rapidly cools down and shrinks and the standard Illarionov and Sunyaev propeller regime [15], with matter outflow from the magnetosphere, is established.

During both spin-up and spin-down, the neutron star angular velocity ω^* almost approaches the angular velocity of matter at the magnetospheric boundary, $\omega^* \rightarrow \omega_m(R_A)$. The difference between ω^* and ω_m is small so the second term in the square brackets in (43) and (44) is much smaller than unity. Also note that when approaching the propeller regime ($R_A \rightarrow R_c$), the accretion rate decreases,

$f(u) \rightarrow 0$, the second term in the square brackets vanishes, and the spin evolution is determined solely by the spin-down term $-\tilde{K}(\theta)\mu^2/R_A^3$. (In the propeller regime, $\omega_m < \omega_K(R_A)$, $\omega_m < \omega^*$, $\omega^* > \omega_K(R_A)$). So the neutron star spins down to the Keplerian frequency at the Alfvén radius. In this regime, the specific angular momentum of the matter that flows in and out from the magnetosphere is, of course, conserved.

Near equilibrium ($\omega^* \sim \omega_m$), relatively small fluctuations in \dot{M} across the shell will lead to very strong fluctuations in $\dot{\omega}^*$ since the toroidal field component can change its sign by changing from $+B_p$ to $-B_p$. If strong coupling actually occurs in nature, this property would be a distinguishing feature of this regime. It is known (see eg. [1], [23]) that real X-ray pulsars sometimes exhibit rapid spin-up/spin-down transitions not associated with X-ray luminosity changes, which may be evidence that they temporarily enter the strong coupling regime. It can not be excluded that the triggering of the strong coupling regime may be due to the magnetic field frozen into the accreting plasma that has not yet entered the magnetosphere. Accretion of magnetized plasma onto neutron stars is studied in detail in the recent work by [24].

3.2 The case of moderate coupling

The strong coupling regime considered above may be realized in the extreme case where the toroidal magnetic field B_t attains a maximum possible value $\sim B_p$ due to magnetic turbulent diffusion. Usually, the coupling of matter with the magnetosphere is mediated by different plasma instabilities whose characteristic times are too short for substantial toroidal field growth. As discussed above in Section 2.1, the shell is very hot close to the magnetosphere boundary, so without cooling above it the plasma is marginally stable with respect to the interchange instability (according to the calculations by [17]).

Let us write down the torque due to magnetic forces applied to the neutron star:

$$I\dot{\omega}^* = \int \frac{B_t B_p}{4\pi} \varpi dS \quad (45)$$

On the other hand, there is a mechanical torque on the magnetosphere from the base of the shell caused by the turbulent stresses $W_{R\phi}$:

$$\int W_{R\phi} \varpi dS, \quad (46)$$

where the viscous turbulent stresses can be written as (see the Appendices for more details)

$$W_{R\phi} = \rho \nu_t R \frac{\partial \omega}{\partial R}. \quad (47)$$

To specify the turbulent viscosity coefficient

$$\nu_t = \langle u_c l_t \rangle, \quad (48)$$

we assume that the characteristic scale of the turbulence close to the magnetosphere is $l_t \sim R_A$, and that the characteristic velocity of the turbulent pulsations is determined by the mechanism of turbulence in the plasma above the magnetosphere. If there are strong convective motions in the shell, caused by heating of its base, then $u_c \sim c_s$, where c_s is the sound speed. If convection is prohibited, there is still turbulence, caused by the shear flow in the shell ($\omega \sim 1/R^2$, see the Appendices). In this case $u_c(R_A) \sim u_\phi(R_A) \sim \omega^* R_A \ll c_s$. Obviously, the ratio of the stresses for the different cases turns out to be of the order of $\omega^*/\omega_K(R_A)$, which for slowly rotating pulsars is around 0.03 – 0.3. Equating the torques (45) and (46), we get

$$\rho u_c R_A \frac{\partial \omega}{\partial R} = \frac{B_t B_p}{4\pi} \quad (49)$$

We eliminate the density from this expression using the pressure balance at the magnetospheric boundary (8) and the expression for the temperature (4), and make the substitution

$$\frac{\partial \omega}{\partial R} = \frac{\omega_m - \omega^*}{\zeta R_A}. \quad (50)$$

Here we have introduced the dimensionless factor $\zeta < 1$, characterizing the size of the zone in which there is an effective exchange of angular momentum between the magnetosphere and the base of the

shell. Then we find the relation between the toroidal and poloidal components of the magnetic field in the magnetosphere:

$$\frac{B_t}{B_p} = \frac{\gamma}{\sqrt{2}(\gamma-1)K_t} \left(\frac{u_c}{u_{ff}} \right) \left(\frac{\omega_m - \omega^*}{\zeta \omega_K(R_A)} \right) \quad (51)$$

(Here and below we have used the following designations: the free fall velocity $u_{ff} \equiv \sqrt{\frac{2GM}{R}}$, the Keplerian frequency at the magnetospheric boundary $\omega_K(R_A)$ and the correction coefficient due to turbulence $K_t \equiv (1 + \gamma m_t^2) \psi(\gamma, m_t)$).

Substituting (51) into (45), in case of convection $u_c = m_c c_s$ (where we have introduced the Mach number for convective motions m_c), the spin-down rate of the neutron star can be written as:

$$I\dot{\omega}^* = \left(\frac{K_1}{\zeta} \right) K_2 \frac{\mu^2}{R_A^3} \frac{\omega_m - \omega^*}{\omega_K(R_A)}. \quad (52)$$

where K_1 is a constant of the order of unity arising from a combination of the parameters in (51). In this case (51) can be re-written in the form

$$\frac{B_t}{B_p} = \tilde{K} \left(\frac{K_1}{\zeta} \right) \frac{\omega_m - \omega^*}{\omega_K(R_A)}, \quad (53)$$

where the geometrical factors arising from the integration of (45) are included in the coefficient $\tilde{K} \sim 1$.

If the differential rotation at the base of the shell gives rise to turbulence, $u_c \sim u_\phi = \omega^* R_A$, and the expression for spin down takes the form

$$I\dot{\omega}^* = \left(\frac{\tilde{K}_1}{\zeta} \right) K_2 \frac{\mu^2}{R_A^3} \left(\frac{R_A}{R_c} \right)^{3/2} \frac{\omega_m - \omega^*}{\omega_K(R_A)}. \quad (54)$$

where

$$R_c \equiv \left(\frac{GM}{\omega^{*2}} \right)^{1/3} \quad (55)$$

is the corotational radius (see also [25]).

Evidently, the breaking torque is in this case smaller by a factor of $(R_A/R_c)^{3/2}$ as compared to when there are convective motions in the shell. We will call this case the case of *weak coupling*. It can easily be seen that in this case both the breaking torque and the spin down rate of the neutron star are independent of the mass accretion rate (in the limit $\omega_m \rightarrow 0$ we have just $K_{sd} \sim \mu^2/R_c^3$, [25]). As will be discussed later on, the non-equilibrium pulsar GX 1+4 shows during spin-down a negative correlation $\dot{\omega}^*$ with luminosity [26]. Therefore, we prefer breaking according to (52) (i.e. with moderate coupling).

Using the definition of the Alfvén radius R_A (11) and the expression for the Keplerian frequency ω_K , we can write (52) in the form

$$I\dot{\omega}^* = Z \dot{M} R_A^2 (\omega_m - \omega^*). \quad (56)$$

Here the dimensionless coefficient Z is

$$Z = \left(\frac{K_1}{\zeta} \right) \frac{\sqrt{2}(\gamma-1)}{f(u)} \frac{K_t}{4\gamma}. \quad (57)$$

Substituting in this formula $\gamma = 5/3$ and the expression (24), we find

$$Z \approx 0.363 \left(\frac{K_1}{\zeta} \right) K_0^{-7/11} K_t^{21/22} \dot{M}_{16}^{-4/11} \mu_{30}^{1/11}. \quad (58)$$

Taking into account that the matter that falls onto the neutron star adds the angular momentum $z \dot{M} R_A^2 \omega^*$ (see Equation (41) above), we get

$$I\dot{\omega}^* = Z \dot{M} R_A^2 (\omega_m - \omega^*) + z \dot{M} R_A^2 \omega^*. \quad (59)$$

It is obvious that for angular momentum removal from the neutron star through a shell, the coefficient Z has to be larger than z . Then the accreting neutron star can episodically spin down (below we will explain this statement in more detail). And conversely, if $Z < z$, the neutron star can only spin up.

If a hot shell is not formed above the magnetosphere (at high X-ray luminosities or low velocity stellar winds, see e.g. [27] and references below), then the supersonic or Bondi accretion regime is established and no angular momentum can be removed from the neutron star. In this case $Z = z$, equation (59) takes the simple form $I\dot{\omega}^* = Z\dot{M}R_A^2\omega_m$, and the neutron star will spin up to a frequency of the order of $\omega_K(R_A)$ regardless of the sign of the difference between the angular momentum of the matter and the magnetic field lines $\omega_m - \omega^*$ close to the magnetospheric boundary. Due to conservation of the specific angular momentum $\omega_m = \omega_B(R_B/R_A)^2$. Without the presence of a shell the evolution of the angular frequency of the neutron star can be described by the equation

$$I\dot{\omega}^* = Z\dot{M}\omega_B R_B^2, \quad (60)$$

where the coefficient Z plays the role of the specific angular momentum of the matter. For example, in the models of [15] $Z \simeq 1/4$. Numerical modeling of Bondi-Hoyle-Littleton accretion in two-dimensional (e.g. [7, 28]) and three-dimensional (e.g. [8, 9]) calculations have, however, shown that due to inhomogeneities in the stellar wind, accretion becomes non-stationary and the sign of the captured angular momentum may change. The sign of Z may thus also be negative and we may observe alternating spin-up and spin-down episodes. Such a scenario is often used to explain the observed changes in the sign of the torque in accreting X-ray pulsars (see the discussion in [29]). We stress again that this picture is completely realistic for X-ray pulsars at high luminosities $> 4 \times 10^{36}$ erg/s, when due to the strong Compton cooling around the rotating magnetosphere no convective quasi-hydrostatic shell can be formed.

If a hot shell is indeed formed (at moderate X-ray luminosities less than $\sim 4 \times 10^{36}$ erg/s, see (34)), the angular momentum from the neutron star can be transferred outside through the convective shell by means of turbulent viscosity. Therefore, substituting ω_m from (36) and (59), we get

$$I\dot{\omega}^* = Z\dot{M}\tilde{\omega}\omega_B R_B^2 \left(\frac{R_A}{R_B}\right)^{2-n} - Z(1 - z/Z)\dot{M}R_A^2\omega^*. \quad (61)$$

This is the main formula that we will use in the following to describe the evolution of the spin of the neutron star.

The dimensionless coefficients in this equation can be calculated using the factor $f(u)$, which is included in the expressions for Z and R_A . Thus, the only dimensionless parameter in the model is $\left(\frac{K_1}{\zeta}\right)$. Below we will show how this coefficient can be determined using observational data from real X-ray pulsars.

4 Spin-up and spin-down of X-ray pulsars

In this section we will study the dependence of the accelerating and decelerating torques on the accretion rate \dot{M} . We would like to stress, again, that in our case accretion is subsonic and the accretion rate is determined by the ability of matter to enter the magnetosphere through the shell. The velocity with which the plasma enters the magnetosphere is then mainly dependent on the density at the magnetospheric boundary. The density distribution in the shell is on the other hand directly connected to the density of matter in the shockwave region and density variations downstream the shock are thus rapidly translated to corresponding variations in the density near the magnetospheric boundary. This means that variations of the accretion rate onto neutron stars in binary systems with circular or low-eccentricity orbits should be essentially independent of orbital phase, and be mostly determined by variations in the stellar wind. In contrast, possible changes in the capture radius R_B (for example due to velocity changes in the stellar wind or variations in the orbital velocity of the neutron star) have little effect on the accretion rate through the shell, but strongly affect the torques applied to the neutron star (see Equation (61)).

Equation (61) can be rewritten in the form explicitly showing spin-up and spin-down torques:

$$I\dot{\omega}^* = A\dot{M}^{\frac{2n+3}{11}} - B\dot{M}^{3/11}. \quad (62)$$

For a characteristic value of the accretion rate $\dot{M}_{16} \equiv \dot{M}/10^{16}$ g/s, the coefficients (not dependent on the accretion rate) will be equal to (in CGS units):

$$A \approx 4.22 \times 10^{31} (0.0388)^{2-n} \tilde{\omega} \left(\frac{K_1}{\zeta}\right) K_0^{-\frac{2n+3}{11}} K_t^{\frac{9+6n}{22}} \mu_{30}^{\frac{13-6n}{11}} \left(\frac{v_8}{\sqrt{\delta}}\right)^{-2n} \left(\frac{P_b}{10\text{d}}\right)^{-1} \quad (63)$$

$$B \approx 5.47 \times 10^{32} (1 - z/Z) \left(\frac{K_1}{\zeta} \right) K_0^{-3/11} K_t^{9/22} \mu_{30}^{13/11} \left(\frac{P^*}{100\text{s}} \right)^{-1} \quad (64)$$

(From now on we will assume $\gamma = 5/3$ in all numerical estimates.) The dimensionless factor $\delta < 1$ takes into account the actual location of the gravitational capture radius, which for a cold stellar wind may be somewhat smaller than the Bondi radius [31]. The capture radius can also be reduced due to radiative heating of the stellar wind by the X-rays from the neutron star (see below). To derive numerical values of the coefficients in Equations (63) and (64), we used the expressions for the coefficient Z (57) using (33) and (31) for the Alfvén radius.

Below we will study the case $Z - z > 0$, i.e. $B > 0$, since in the opposite case only spin-up of the neutron star is possible.

4.1 Equilibrium pulsars

For equilibrium pulsars we set $\dot{\omega}^* = 0$ and from Equation (59) we get

$$Z_{eq}(\omega_m - \omega^*) + z\omega^* = 0. \quad (65)$$

Close to equilibrium we may vary (59) with respect to \dot{M} . It is convenient to introduce the dimensionless parameter $y \equiv \dot{M}/\dot{M}_{eq}$, so that close to equilibrium $y = 1$. Variations in $\delta\dot{M}$ may in general be caused by changes in density $\delta\rho$ as well as in velocity of the stellar wind δv (and thus the Bondi radius). From the continuity equation and taking into account the dependence of $f(u)$ on \dot{M} in the shell (33), we get

$$\frac{7}{11} \frac{\delta\dot{M}}{\dot{M}} = \frac{\delta\rho}{\rho} - 3 \frac{\delta v}{v} \quad (66)$$

Let us start by studying variations in the density only. Assuming $R_B = \text{const}$, we find

$$I \frac{\partial \dot{\omega}^*}{\partial \dot{M}} \Big|_{eq} = I \frac{1}{\dot{M}_{eq}} \frac{\partial \dot{\omega}^*}{\partial y} \Big|_{y=1} = \frac{4}{11} z \omega^* R_A^2 + \frac{2n}{11} Z_{eq} \omega_m R_A^2 \quad (67)$$

Using the expression for ω_m from (65) and substituting it into (67), we get

$$Z_{eq,\rho} - \frac{n-2}{n} z = \frac{I \frac{\partial \dot{\omega}^*}{\partial \dot{M}} \Big|_{eq}}{\frac{2n}{11} \omega^* R_A^2} \approx \frac{3.64}{n} \left(\frac{\frac{\partial \dot{\omega}^*}{\partial y} \Big|_{y=1}}{10^{-12}} \right) \left(\frac{P^*}{100\text{s}} \right) K_0^{-4/11} K_T^{6/11} \dot{M}_{16}^{-7/11} \mu_{30}^{-12/11}. \quad (68)$$

Now let us keep the density constant and study changes in the velocity only. Then, we have from (66) that $\delta v/v = -(7/33)\delta\dot{M}/\dot{M}$. Varying (59), we get

$$Z_{eq,v} - \frac{5n-3}{5n} z = \frac{I \frac{\partial \dot{\omega}^*}{\partial \dot{M}} \Big|_{eq}}{\frac{20n}{33} \omega^* R_A^2} \approx \frac{1.1}{n} \left(\frac{\frac{\partial \dot{\omega}^*}{\partial y} \Big|_{y=1}}{10^{-12}} \right) \left(\frac{P^*}{100\text{s}} \right) K_0^{-4/11} K_T^{6/11} \dot{M}_{16}^{-7/11} \mu_{30}^{-12/11}. \quad (69)$$

A majority of neutron stars in X-ray pulsars rotate close to their equilibrium periods, i.e. on average $\dot{\omega}^* = 0$. Near equilibrium we get from (62) in the settling accretion regime:

$$\mu_{30}^{(eq)} \approx \left(\frac{0.077 \cdot (0.0388)^{(2-n)} \tilde{\omega}}{1 - z/Z} \right)^{\frac{11}{6n}} K_0^{-1/3} K_t^{1/2} \left(\frac{\sqrt{\delta}}{v_8} \right)^{\frac{11}{3}} \dot{M}_{16}^{1/3} \left(\frac{P_*/100\text{s}}{P_b/10?} \right)^{\frac{11}{6n}}. \quad (70)$$

This expression can be reversed to give the equilibrium period for a system if the magnetic field is known:

$$P_{eq} \approx \frac{1300[\text{s}]}{0.0388^{2-n}} (1 - z/Z_{eq}) \tilde{\omega}^{-1} K_0^{2n/11} K_t^{-3n/11} \mu_{30,eq}^{6n/11} \left(\frac{P_b}{10\text{d}} \right) \dot{M}_{16}^{-2n/11} \left(\frac{v_8}{\sqrt{\delta}} \right)^{2n}. \quad (71)$$

The ratio of pulsar's to Keplerian frequency at the Alfvén radius is independent of n and equal to

$$\frac{\omega^*}{\omega_K(R_A)} \approx 0.27 K_0^{3/11} K_t^{-9/22} \left(\frac{P^*}{100\text{s}} \right)^{-1} \mu_{30}^{9/11} \dot{M}_{16}^{-3/11}. \quad (72)$$

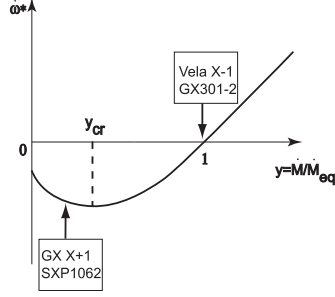


Figure 2: An illustration of the dependence of $\dot{\omega}^*$ on the dimensionless accretion rate y [(82)]. In fact as $y \rightarrow 0$, $\dot{\omega}^*$ approaches some negative value since the neutron star enters the propeller regime at small accretion rates. The figure shows the position in the diagram for equilibrium pulsars with $y \sim 1$ and for non-equilibrium pulsars at steady spin-down with $y < y_{cr}$

At equilibrium, the ratio between the toroidal and poloidal magnetic fields at the Alfvén radius (Equation (51)) takes the form:

$$\frac{B_t}{B_p}|_{eq} = - \left(\frac{K_1}{\zeta} \right) \left(\frac{z}{Z_{eq}} \right) \left(\frac{\omega^*}{\omega_K(R_A)} \right) = \frac{10f(u)z}{\sqrt{2}K_t} \left(\frac{\omega^*}{\omega_K(R_A)} \right). \quad (73)$$

Substituting $f(u)$ and (72) in this expression, we get:

$$\left| \frac{B_t}{B_p} \right|_{eq} \approx 0.75z \frac{K_0^{10/11}}{K_t^{15/11}} \left(\frac{P^*}{100s} \right)^{-1} \mu_{30}^{8/11} \dot{M}_{16}^{1/11} \quad (74)$$

We stress that for slowly rotating accreting pulsars the ratio between the neutron star spin frequency and the Keplerian frequency at the Alfvén radius is always smaller than unity. Therefore, for typical values $f(u) \sim 0.3$ and $z = 2/3$ we have $B_t/B_p < 1.5(\omega^*/\omega_K(R_A)) < 1$, and the pulsars are far from being in the propeller regime (see further discussion in Section 6.2).

We would like to stress that in the important case $n = 2$ (iso-angular-momentum distribution), the coefficient in the second term in (68) vanishes, and thus equating Z_{eq} to (58) we find the value of the magnetic moment of the neutron star only from the pulsar equilibrium period and the derivative $(\partial\dot{\omega}/\partial y)_{eq}$:

$$\mu_{30,eq} \approx 5 \left(\frac{\partial\dot{\omega}^*}{\partial y}|_{y=1} \right) \left(\frac{P^*}{100s} \right) \left(\frac{K_1}{\zeta} \right)^{-1} K_0^{3/11} K_t^{-3/7} \dot{M}_{16}^{-3/11}. \quad (75)$$

For the case $n = 2$ and a known μ_{eq} we obtain the stellar wind velocity:

$$\frac{v_8}{\sqrt{\delta}} \approx 0.53(1 - z/Z_{eq})^{-1/4} K_0^{-1/11} K_t^{3/22} \dot{M}_{16}^{1/11} \mu_{30,eq}^{-3/11} \left(\frac{P^*/100s}{P_b/10d} \right)^{1/4}. \quad (76)$$

As will be shown below, for real equilibrium pulsars $z/Z_{eq} \ll 1$, and thus the derived formula gives a correct estimate of the stellar wind velocity. Note the weak dependence of the formula on the dimensionless constant as well as on the accretion rate. In the framework of our model we may thus, with knowledge of the equilibrium spin period P^* , the binary period P_b and with an estimate of the neutron star magnetic field μ , determine the stellar wind velocity, without complicated spectroscopic measurements.

4.2 Non-equilibrium pulsars

Below we will study the case $Z - z > 0$, and thus $B > 0$, since in the opposite case only spin-up is possible.

First of all, we note that the function $\dot{\omega}^*(\dot{M})$ reaches a minimum for some \dot{M}_{cr} . Differentiating equation (62) with respect to \dot{M} and equating the achieved expression to zero, we find

$$\dot{M}_{cr} = \left[\frac{B}{A} \frac{3}{(3 + 2n)} \right]^{\frac{11}{2n}}. \quad (77)$$

For $\dot{M} = \dot{M}_{cr}$ the expression $\dot{\omega}^*$ reaches an absolute minimum (see. Fig.2).

It is convenient to introduce the dimensionless parameter

$$y \equiv \frac{\dot{M}}{\dot{M}_{eq}} \quad (78)$$

where \dot{M}_{eq} represents the accretion rate at which $\dot{\omega}^* = 0$:

$$\dot{M}_{eq} = \left(\frac{B}{A}\right)^{11/2n} \quad (79)$$

Obviously,

$$\dot{M}_{cr} = \dot{M}_{eq} \left(\frac{3}{2n+3}\right)^{\frac{11}{2n}}, \quad (80)$$

In other words, $\dot{\omega}^*$ has a minimum for a value of the dimensionless parameter of

$$y_{cr} = \left(\frac{3}{2n+3}\right)^{\frac{11}{2n}} < 1. \quad (81)$$

Equation (62) can be rewritten in the form

$$I\dot{\omega}^* = A\dot{M}_{eq}^{\frac{3+2n}{11}} y^{\frac{3+2n}{11}} \left(1 - y^{-\frac{2n}{11}}\right), \quad (82)$$

The minimum $\dot{\omega}^*$ for $y = y_{cr}$ (i.e. the maximum possible spin-down rate of the pulsar) is

$$I\dot{\omega}_{min}^* = -\frac{2n}{3} A\dot{M}_{eq}^{\frac{3+2n}{11}} y^{\frac{3+2n}{11}}. \quad (83)$$

Now, we vary (82) with respect to y :

$$I\delta\dot{\omega}^* = I\frac{\partial\dot{\omega}^*}{\partial y}(\delta y) = \frac{3}{11} A\dot{M}_{eq}^{\frac{3+2n}{11}} y^{-8/11} \left(\frac{2n+3}{3} y^{\frac{2n}{11}} - 1\right) (\delta y). \quad (84)$$

Apparently, depending on whether $y > y_{cr}$ or $y < y_{cr}$, *correlated changes* of $\delta\dot{\omega}^*$ with X-ray flux should have different signs. Indeed, for GX 1+4 in [26] and [32] a positive correlation of the observed δP with $\delta\dot{M}$ was found using the CGRO *BATSE* and *Fermi* GBM data. This means that there is a negative correlation between $\delta\dot{\omega}^*$ and $\delta\dot{M}$, suggesting $y < y_{cr}$ in this source.

Let us now consider accreting pulsars in the stage of spin-down (like e.g. GX 1+4 and SXP 1062). If the pulsar is spinning down, measurements of the spin-down rate give limits on the parameters of our model. From the simple fact that the spin down is stable, using equations (62), (63) and (64) we may obtain a lower limit on the magnetic field in the case of quasi-spherical accretion with $\dot{\omega}^* < 0$,

$$\mu_{30} > \mu_{30,min} \approx 0.1(1 - z/Z)^{-\frac{11}{12}} \dot{\omega}^{\frac{11}{12}} K_0^{-1/3} K_t^{1/2} \left(\frac{\sqrt{\delta}}{v_8}\right)^{\frac{11}{3}} \dot{M}_{16}^{1/3} \left(\frac{P_*/100s}{P_b/10d}\right)^{\frac{11}{12}} \quad (85)$$

(and thus equation (70) is here transformed into an inequality). We now make use of the fact that during spin down there is a maximum possible breaking torque (see equation (83)). Inserting the values of the coefficients A and B from equations (63) and (64) into (83), we find:

$$\dot{\omega}_{sd,max}^* \approx -1.13 \times 10^{-12} [\text{rad/s}] (1 - z/Z)^{7/4} \left(\frac{K_1}{\zeta}\right) \mu_{30}^2 \left(\frac{v_8}{\sqrt{\delta}}\right)^3 \left(\frac{P^*}{100s}\right)^{-7/4} \left(\frac{P_b}{10d}\right)^{3/4}. \quad (86)$$

For the accretion rate $\dot{M} = \dot{M}_{cr}$ this expression reaches the numerical value

$$\dot{M}_{16,cr} \approx 112(1 - z/Z)^{11/4} K_0 K_t^{-2} \mu_{30}^3 \left(\frac{v_8}{\sqrt{\delta}}\right)^{11} \left(\frac{P_b/10d}{P_*/100s}\right)^{\frac{11}{4}}. \quad (87)$$

(Note the extremely strong dependence on the stellar wind velocity.)

Then, from the condition $|\dot{\omega}_{sd}^*| \leq |\dot{\omega}_{sd,max}^*|$ follows a more interesting lower limit on the neutron star magnetic field:

$$\mu_{30} > \mu'_{30,min} \approx 0.94 \left| \frac{\dot{\omega}_{sd}^*}{10^{-12}\text{rad/s}} \right| \left(\frac{K_1}{\zeta} \right)^{-1/2} \left(\frac{v_8}{\sqrt{\delta}} \right)^{-3/2} \left(\frac{P^*}{100\text{s}} \right)^{7/8} \left(\frac{P_b}{10\text{d}} \right)^{-3/8}. \quad (88)$$

Note the weaker dependence of this estimate on the stellar wind velocity as compared to the inequality (85).

If the accelerating torque can be neglected compared to the breaking torque (corresponding to the low X-ray luminosity limit $y \ll 1$), we find directly from (52) that for accreting pulsars at spin down,

$$\dot{\omega}_{sd}^* \approx -0.55 \times 10^{-12} [\text{rad/s}] \left(\frac{K_1}{\zeta} \right) K_0^{-3/11} K_t^{9/22} \mu_{30}^{13/11} \dot{M}_{16}^{3/11} \left(\frac{P^*}{100\text{s}} \right)^{-1}. \quad (89)$$

From this we obtain a lower limit on the neutron star magnetic field that does not depend on the parameters of the stellar wind nor the binary orbital period:

$$\mu_{30} > \mu''_{30,min} \approx 1.66 \left| \frac{\dot{\omega}_{sd}^*}{10^{-12}\text{rad/s}} \right|^{11/13} \left(\frac{K_1}{\zeta} \right)^{-11/13} K_0^{3/13} K_t^{-9/26} \dot{M}_{16}^{-3/13} \left(\frac{P^*}{100\text{s}} \right)^{11/13}. \quad (90)$$

Eliminating $\left(\frac{K_1}{\zeta} \right)$ from (53) and (52) we get:

$$\left| \frac{B_t}{B_p} \right| = \tilde{K} \left| \frac{I \dot{\omega}_{sd}^* R_A^3}{K_2 \mu^2} \right| \approx 0.49 \left| \frac{\dot{\omega}_{sd}^*}{10^{-12}\text{rad/s}} \right| \mu_{30}^{-4/11} K_0^{-6/11} K_t^{-9/11} \dot{M}_{16}^{-6/11}. \quad (91)$$

We see from (91), that with decreasing \dot{M} the ratio B_t/B_p increases for reasons well understood — at low \dot{M} the characteristic cooling time for the plasma increases and the toroidal component has time to grow to the same strength as the poloidal. B_t can, however, not become larger than B_p due to an instability similar to that of a tightly wound spring. Equating $B_t = B_p$, and using (91), we find the luminosity below which the pulsar enters the strong coupling regime during spin down (see Section 3.1 above):

$$\dot{M}_{16}^* \approx 0.27 \left| \frac{\dot{\omega}_{sd}^*}{10^{-12}\text{rad/s}} \right|^{11/6} \mu_{30}^{-2/3} K_0 K_t^{-3/2}. \quad (92)$$

Below this luminosity in the strong coupling regime the spin-down law becomes $K_{sd} \sim \mu^2 R_A^{-3} \sim \dot{M}^{6/11}$:

$$\dot{\omega}_{sd}^* \approx -2 \times 10^{-12} [\text{rad/s}] \mu_{30}^{4/11} K_0^{-6/11} K_t^{9/11} \dot{M}_{16}^{6/11} \quad (93)$$

(Note that when the spin-up torque can be neglected the expression does not contain the - ever so hard to determine - velocity of the stellar wind.)

For a further decrease of the accretion rate in non-equilibrium pulsars, the Alfvén radius will grow to the corotation radius and the pulsar may enter a transient state (the propeller regime). From the condition $\omega^* = \sqrt{GM/R_A^3}$ we find the accretion rate for this transition:

$$\dot{M}_{16}^{**} \approx 0.0082 K_0 K_t^{-3/2} \mu_{30}^3 \left(\frac{P^*}{100\text{s}} \right)^{-11/3}. \quad (94)$$

The formulae derived above show that the restrictions on the model become more significant if the neutron star magnetic field can be measured independently (for example using spectral cyclotron lines). We also would like to stress the fact that measurements of correlated fluctuations of the spin frequency derivative with luminosity during spin down allows us to place the source in a $\dot{\omega}^* - y$ diagram (see Fig. 2). To the right from the minimum $y > y_{cr}$ and the correlation positive. To the left $y < y_{cr}$ and the correlation is negative. This way we may obtain further limits on the parameters of our model. Below we will perform this analysis for the source GX 1+4, in which such correlations where measured [26], [32].

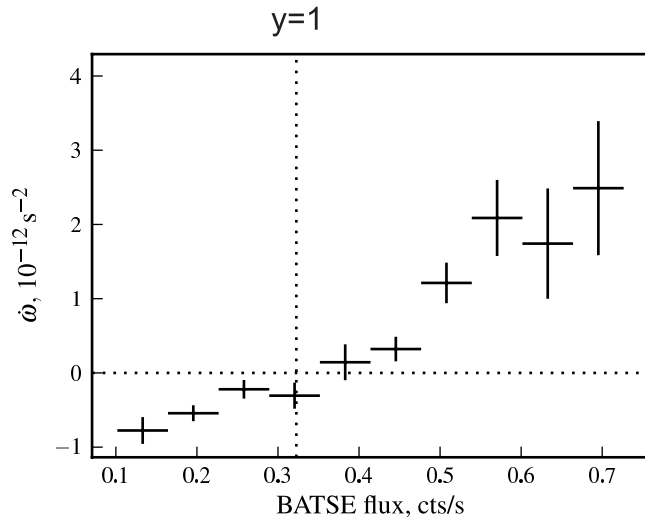


Figure 3: Torque-luminosity correlation in GX 301-2, $\dot{\omega}^*$ as a function of BATSE data (20-40 keV pulsed flux) near the equilibrium frequency, see [47]. The assumed X-ray flux at equilibrium (in terms of the dimensionless parameter y) is also shown by the vertical dotted line.

5 Application to real X-ray pulsars

In this Section, as an illustration of the possible applicability of our model to real sources, we will consider five particular slowly rotating moderately luminous X-ray pulsars: GX 301-2, Vela X-1, GX 1+4, SXP 1062 and 4U 2204+56. The first two pulsars are close to the equilibrium rotation of the neutron star, showing spin-up/spin-down excursions near the equilibrium frequency (apart from the spin-up/spin-down jumps, which may be, we think, due to episodic switch-ons of the strong coupling regime when the toroidal magnetic field component becomes comparable to the poloidal one, see Section 3.1). The third source, GX 1+4, is a typical example of a pulsar displaying long-term spin-up/spin-down episodes. During the last 30 years, it has shown a steady spin-down with frequency fluctuations (anti-)correlated with luminosity (see [32] for a more detailed discussion). Clearly, this pulsar can not be considered to be in equilibrium. The pulsar SXP 1062 in the Large Magellanic Cloud as well as the pulsar 4U 2206+54 have only been observed at steady spin-down.

5.1 GX 301-2

GX301-2 (also known as 4U 1223-62) is a high-mass X-ray binary, consisting of a neutron star and an early type B optical companion with mass $\simeq 40M_{\odot}$ and radius $\simeq 60R_{\odot}$. The binary period is 41.5 days [39]. The neutron star is a ~ 680 s X-ray pulsar [40], accreting from the strong wind of its companion ($\dot{M}_{loss} \sim 10^{-5}M_{\odot}/\text{yr}$, [41]). The photospheric escape velocity of the wind is $v_{esc} \approx 500$ km/s. The semi-major axis of the binary system is $a \approx 170R_{\odot}$ and the orbital eccentricity $e \approx 0.46$. The wind terminal velocity was found [41] to be about 300 km/s, smaller than the photospheric escape velocity.

GX 301-2 shows strong short-term pulse period variability, which, as in many other wind-accreting pulsars, can be well described by a random walk model [42]. Earlier observations between 1975 and 1984 showed a period of ~ 700 s while in 1984 the source started to spin up [43]. The almost 10 years of spin-up were followed by a reversal of spin in 1993 [44] after which the source has been continuously spinning down [45], [46], [47]. Rapid spin-up episodes sometimes appear in the *Fermi* GBM data on top of the long-term spin-down trend [23]. It can not be excluded that these rapid spin-up episodes, as well as similar ones observed in BATSE data, reflect a temporary entrance into the strong coupling regime, as discussed in Section 2.4.1. Cyclotron line measurements [45] yield a magnetic field estimate near the neutron star surface of $B_0 \approx 4.4 \times 10^{12}$ G ($\mu = 1/2B_0R_0^3 = 2.2 \times 10^{30}$ G cm³ for the assumed neutron star radius $R_0 = 10$ km).

In Fig. 3 we have plotted $\dot{\omega}^*$ as a function of the observed pulsed flux (20-40 keV) according to BATSE data (see [47] for more detail). We will consider the neutron star magnetic field in this source to

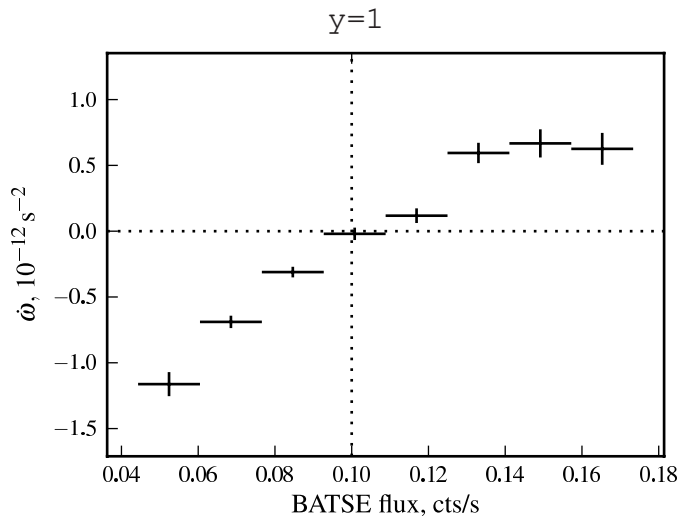


Figure 4: The same as in Fig. 3 for Vela X-1 [55].

be known from observations. An estimate of \dot{M} can be inferred from the X-ray flux provided the distance to the source is known, which is generally not the case to a great certainty. We shall assume that near equilibrium a hot quasi-spherical shell exists in this pulsar and that the accretion rate is 3×10^{16} g/s, i.e. not higher than the critical value $\dot{M}_* \simeq 4 \times 10^{16}$ g/s [(34)]. The derivative $\partial\dot{\omega}^*/\partial y$ can be derived from the $\dot{\omega}^* - \text{X-ray flux}$ plot, since in the first approximation the accretion rate is proportional to the observed pulsed X-ray flux. Near the equilibrium (the torque reversal point with $\dot{\omega}^* = 0$), we find from a linear fit in Fig. 3 $\partial\dot{\omega}^*/\partial y \approx 1.5 \times 10^{-12}$ rad/s².

The obtained parameters (Z , $\left(\frac{K_1}{\zeta}\right)$ etc.) for this pulsar are listed in Table 1. We note that the toroidal component of the magnetic field is much less than the poloidal (the pulsar is far from the strong-coupling limit). The stellar wind velocity, determined using the formula (76), is close to the photospheric escape velocity. We also note that the value of the parameter describing the coupling between the plasma and the magnetosphere K_1/ζ is of the order of 14, although by its physical sense the coefficient K_1 should be of the order of 1. This means that the value of the parameter ζ , which gives the characteristic relative size of the region in which transfer of angular momentum from the shell takes place to the magnetosphere (or vice versa) has to be of the order of 1/10 (i.e. the characteristic size of the region where angular momentum transfer takes place should be approximately 1/10 of the Alfvén radius).

5.2 Vela X-1

Vela X-1 (=4U 0900-40) is the brightest persistent accretion-powered pulsar in the 20-50 keV energy band with an average luminosity of $L_x \approx 4 \times 10^{36}$ erg/s [43]. It consists of a massive neutron star ($1.88 M_\odot$, [48]) and the B0.5Ib super giant HD 77581, which eclipses the neutron star every orbital cycle of ~ 8.964 days [49]. The neutron star was discovered as an X-ray pulsar with a spin period of ~ 283 s [50], which has remained almost constant since the discovery of the source. The optical companion has a mass and radius of $\sim 23 M_\odot$ and $\sim 30 R_{sun}$ respectively [49]. The photospheric escape velocity is $v_{esc} \approx 540$ km/s. The orbital separation is $a \approx 50 R_\odot$ and the orbital eccentricity $e \approx 0.1$. The primary almost fills its Roche lobe (as also evidenced by the presence of elliptical variations in the optical light curve, [51]). The mass-loss rate from the primary star is $10^{-6} M_\odot/\text{yr}$ (Nagase et al. 1986) via a fast wind with a terminal velocity of ~ 1100 km/s [53], which is typical for this class. Despite the fact that the terminal velocity of the wind is rather large, the compactness of the system makes it impossible for the wind to reach this velocity before interacting with the neutron star, so the relative velocity of the wind with respect to the neutron star is rather low, ~ 700 km/s.

Cyclotron line measurements [54] yield the magnetic field estimate $B_0 \approx 3 \times 10^{12}$ G ($\mu = 1.5 \times 10^{30}$ G cm³ for the assumed neutron star radius 10 km). We shall assume that in this pulsar $\dot{M} \simeq 3 \times 10^{16}$ g/s (again for the existence of a shell to be possible). In Fig. 4 we have plotted $\dot{\omega}^*$ as a function of the

observed pulsed flux (20-40 keV) according to BATSE data [55]. As in the case of GX 301-2, from a linear fit we find at the spin-up/spin-down transition point $\partial\dot{\omega}^*/\partial y \approx 1.2 \times 10^{-12}$ rad/s².

The obtained parameters for Vela X-1 are listed in Table 1. We note that the velocity of the stellar wind as obtained using (76) is very close to the observed value of 700 km/s. As in the case of GX 1+4, the value of the coupling parameter K_1/ζ is of the order of 10, i.e. the size of the region for transfer of angular momentum between the plasma and the magnetosphere is about 1/10 of the Alfvén radius.

5.3 GX 1+4

GX 1+4 was the first source to be identified as a symbiotic binary containing a neutron star [56]. The pulse period is ~ 140 s and the donor is an MIII giant [56]. The system has an orbital period of 1161 days [57], making it the widest known LMXB by at least one order of magnitude. The donor is far from filling its Roche lobe and accretion onto the neutron star is by capture of the stellar wind of the companion.

The system has a very interesting spin history. During the 1970's it was spinning up at the fastest rate ($\dot{\omega}_{su} \sim 3.8 \cdot 10^{-11}$ rad/s) among the known X-ray pulsars at the time (e.g. [43]). After several years of non-detections in the early 1980's, it reappeared again, now spinning down at a rate similar in magnitude to that of the previous spin-up. At present the source is steadily spinning down with an average spin down rate of $\dot{\omega}_{sd} \approx -2.34 \times 10^{-11}$ rad/s. The observed spin-reversal has been interpreted in terms of a retrograde accretion disc forming in the system [58], [59], [26]. A detailed spin-down history of the source is discussed in the recent paper [32]. Using our model this behavior can, however, be readily explained in the framework of quasi-spherical accretion.

As the pulsar in GX 1+4 is not in equilibrium, we use one of the three formulas from Section 4.2 to derive a lower limit on the neutron star magnetic field from the observed value of $\dot{\omega}_{sd}$. From (88) we get $\mu'_{30,min} \approx 12(K_1/\zeta)^{-1/2}$. Assuming that the coupling parameter for non-equilibrium pulsars is similar to that in equilibrium ones (and thus that the size of the region where transfer of angular momentum between the plasma and the magnetosphere takes place is of the order of 1/10 of the Alfvén radius, $\zeta \sim 0.1$) we find that $\mu'_{30,min} \sim 4$.

In this source we also observe anti-correlated variability in spin-down rate versus X-ray luminosity [26]. According to the latest *Fermi* GBM data in the paper [32] it was found that $-\dot{\omega}^* \sim L_x^{0.3}$. In our model for moderate coupling, $K_{sd} \sim \dot{M}^{3/11}$, which is very similar to the observed relation. In the earlier *BATSE* observations [26] it was found that $-\dot{\omega}^* \sim L_x^{0.48}$. It can not be excluded that the average luminosity of the source was lower at this time. In that case the component B_t could have been closer to B_p , and then the expected correlation would have had the form $K_{sd} \sim \dot{M}^{6/11} \sim L_x^{0.54}$. Note that in the model with weak coupling (with transfer of angular momentum due to turbulence close to the magnetosphere [25]), the breaking torque is less effective by a factor of $(R_A/R_c)^{3/2}$ and not at all dependent on the luminosity. In low-luminosity pulsars the cooling close to the Alfvén radius is less effective, which leads to the development of convective movements in the shell and the establishment of the moderate coupling regime.

Further, we note that the short-term spin-up episodes, sometimes observed on top of the steady spin-down behaviour (at about MJD 49700, see Fig. 2 in [26]) are correlated with an enhancement of the X-ray flux, in contrast to the negative frequency-flux correlations discussed above. During these short spin-ups, $\dot{\omega}^*$ is about half the average $\dot{\omega}_{su}^*$ observed during the steady spin-up state of GX 1+4 up to 1980. The X-ray luminosity during these episodic spin-ups is approximately five times larger than the mean X-ray luminosity during the steady spin-down. We remind the reader that once $\dot{M} > \dot{M}_*$, a free-fall gap appears above the magnetosphere, and the neutron star can only spin up. When the X-ray flux drops again, the settling accretion regime is re-established and the neutron star resumes its spinning-down.

5.4 SXP 1062

This recently discovered young X-ray pulsar in Be/X-ray binary system, located in a supernova remnant in the Small Magellanic Cloud. Its rotational period is $P^* \approx 1062$ s and it has a low X-ray luminosity of $L_x \approx 6 \times 10^{35}$ erg/s [60]. The source shows a remarkably high spin-down rate of $\dot{\omega}^* \approx -1.6 \times 10^{-11}$ (rad/s²). Its origin is widely discussed in the literature (see e.g. [61], [37]) and a possibly anomalously high magnetic field of the neutron star has been suggested [63]. In the framework of our model we use more conservative limits. Neglecting the spin-up torque (90), we get $\mu_{30} > \mu''_{30,min} \approx 20$. This shows that the observed spin down can be explained by a magnetic field of the order of 10^{13} G, and thus we believe it is premature to conclude that the source is an accreting magnetar.

Table 1: Parameters for the pulsars discussed in Section 5. References for the observed pulsar and orbital parameters are given in the text as well as values for the wind velocities from measurements of the optical components. The parameters Z , K_1/ζ and $f(u)$ were derived in Sections 2.3 and 3. Numerical estimates are given assuming iso-angular-momentum rotation in the shell ($n = 2$), moderate coupling between the plasma and the magnetic field $\delta = 1, \zeta = 1, \tilde{\omega} = 1, K_0 = 1, \gamma = 5/3$ without turbulence ($m_t = 0, K_t = 1$).

Pulsars	equilibrium pulsars		non-equilibrium pulsars		
	GX301 – 2	VelaX – 1	GX1 + 4	SXP1062	4U2206 + 54
Measured parameters					
$P^*(\text{s})$	680	283	140	1062	5560
$P_B(\text{d})$	41.5	8.96	1161	$\sim 300^\dagger$	19
$v_w(\text{km/s})$	300	700	200	$\sim 300^\ddagger$	350
μ_{30}	2.7	1.2	?	?	1.7
\dot{M}_{16}	3	3	1	0.6	0.2
$\frac{\partial \dot{\omega}}{\partial y} _{y=1}(\text{rad/s}^2)$	$1.5 \cdot 10^{-12}$	$1.2 \cdot 10^{-12}$	n/a	n/a	n/a
$\dot{\omega}_{sd}^*$	0	0	$-2.34 \cdot 10^{-11}$	$-1.63 \cdot 10^{-11}$	$-9.4 \cdot 10^{-14}$
Derived parameters					
$f(u)$	0.53	0.57			
$\left(\frac{K_1}{\zeta}\right)$	14	10			$\gtrsim 8$
Z	3.7	2.6			
B_t/B_p	0.17	0.22			
$R_A(\text{cm})$	$2 \cdot 10^9$	$1.4 \cdot 10^9$			
$\omega^*/\omega_K(R_A)$	0.07	0.08			
$v_{w,min}(\text{km/s})$	500	740			
$\mu_{30,min}$			$\mu'_{min} \approx 4$	$\mu''_{min} \approx 20$	$\mu'_{min} \approx 3.6$

[†] Estimate of the source's position in the Corbet diagram [‡] Estimate of typical wind velocity binary pulsars containing Be-stars.

5.5 4U 2204+56

This slowly rotating pulsar has a period of $P^* = 5560$ s and shows a spin-down rate of $\dot{\omega}_{sd} \approx -9.4 \times 10^{-14}$ rad/s [64]. The orbital period of the binary system is $P_b \simeq 19$ days [64], and the measured stellar wind velocity is $v_W \approx 350$ km/s, abnormally low for an O9.5V [65] optical counterpart. The X-ray luminosity of the source is on average $L_x \simeq 2 \times 10^{35}$ erg/s. A feature in the X-ray spectrum sometimes observed around 30 keV can be interpreted as a cyclotron line [66], [67], [68], [69]. That gives an estimate of the magnetic field of the order of $B \sim (30/11.6) \times 1.3 \approx 3.4 \times 10^{12}$ G (taking into account the gravitational redshift close to the surface $1 + z \sim 1.3$), and thus $\mu_{30} \approx 1.7$. Using this value of the magnetic field and neglecting the accelerating torque, from the formula in (89) we obtain a lower limit on the parameter $K_1/\zeta \gtrsim 8$, which is very close to the coupling parameter values for the equilibrium pulsars Vela X-1 and GX 301-2. If we consider the magnetic field to be unknown (see discussion in [64]), and apply the formula(88), like in the case of GX 1+4, assuming moderate coupling with $K_1/\zeta \sim 10$, we get the limit $\mu_{30} > \mu'_{30,min} \approx 3.6$, which is in agreement with standard neutron star magnetic field values. Note that using our formulas for equilibrium pulsars would here give a magnetar value for the magnetic field [64].

6 Discussion

6.1 Physical conditions inside the shell

For an accretion shell to be formed around the neutron star magnetosphere it is necessary that the matter crossing the bow shock does not cool down too rapidly and thus starts to fall freely. This means that the radiation cooling time t_{cool} must be longer than the characteristic time of plasma motion.

The plasma is heated up in the strong shock to a temperature

$$T_{ps} = \frac{3}{16} \mu_m \frac{v_w^2}{\mathcal{R}} \approx 1.36 \times 10^5 [\text{K}] \left(\frac{v_w}{100 \text{ km/s}} \right)^2. \quad (95)$$

The radiative cooling time of the plasma is

$$t_{cool} = \frac{3kT}{2\mu_m n_e \Lambda} \quad (96)$$

where ρ is the plasma density, $n_e = Y_e \rho / m_p$ is the electron number density ($\mu_m = 0.6$ and $Y_e \approx 0.8$ for fully ionized plasma with solar abundance). Λ is the cooling function which can be approximated as

$$\Lambda(T) = \begin{cases} 0, & T < 10^4 \text{ K} \\ 1.0 \times 10^{-24} T^{0.55}, & 10^4 \text{ K} < T < 10^5 \text{ K} \\ 6.2 \times 10^{-19} T^{-0.6}, & 10^5 \text{ K} < T < 4 \times 10^7 \text{ K} \\ 2.5 \times 10^{-27} T^{0.5}, & T > 4 \times 10^7 \text{ K} \end{cases} \quad (97)$$

[70], [71].

Compton cooling becomes effective from the radius where the gas temperature T , determined by the hydrostatic formula (4), is lower than the X-ray Compton temperature T_x . The Compton cooling time (see (17)) is:

$$t_C \approx 1060 [\text{s}] \dot{M}_{16}^{-1} \left(\frac{R}{10^{10} \text{ cm}} \right)^2. \quad (98)$$

Above the radius where $T_x = T$, Compton heating dominates. Taking the actual temperature close to the adiabatic one [(4)], we find $R_x \approx 2 \times 10^{10}$ cm. We note that both the Compton and photoionization heating processes are controlled by the photoionization parameter ξ [72], [73]

$$\xi = \frac{L_x}{n_e R^2}. \quad (99)$$

In most part of the accretion flux, $n \sim R^{-3/2}$, so $\xi \sim R^{-1/2}$ and independent of the X-ray luminosity through the mass continuity equation. We derive a characteristic value for ξ :

$$\xi \approx 5 \times 10^5 f(u) R_{10}^{-1/2}. \quad (100)$$

If Compton processes were effective everywhere, this high value of the parameter ξ would imply that the plasma is Compton-heated up to keV-temperatures out to very large distances $\sim 10^{12}$ cm. However, at large distances the Compton heating time becomes longer than the characteristic time of gas accretion:

$$\frac{t_C}{t_{accr}} = \frac{t_C f(u) u_{ff}}{R} \approx 20 f(u) \dot{M}_{16}^{-1} R_{10}^{1/2}, \quad (101)$$

which shows that Compton heating is ineffective. The gas temperature is determined by photoionization heating only and the gas can only be heated up to $T_{max} \approx 5 \times 10^5$ K [72], which is substantially lower than $T_x \sim 3$ keV.

The effective gravitational capture radius corresponding to the sound velocity of the gas in the photoionization-heated zone is

$$R_B^* = \frac{2GM}{c_s^2} = \frac{2GM}{\gamma \mathcal{R} T_{max} / \mu_m} \approx 3.5 \times 10^{12} \text{cm} \left(\frac{T_{max}}{5 \times 10^5 \text{K}} \right)^{-1}. \quad (102)$$

Everywhere up to the bow shock photoionization keeps the temperature at a value $\simeq T_{max}$. The sound velocity corresponding to T_{max} is approximately 80 km/s. If the stellar wind velocity exceeds 80 km/s, a standard bow shock is formed at the Bondi radius with a post-shock temperature given by (95). If the stellar wind velocity is lower than this value, the shock disappears and quasi-spherical accretion occurs from R_B^* . The photoionization heating time at the effective Bondi radius 3×10^{12} cm is

$$t_{pi} \approx \frac{(3/2)kT_{max}/\mu_m}{(h\nu_{eff} - \zeta_{eff})n_\gamma \sigma_{eff} c} \approx 2 \times 10^4 [\text{s}] \dot{M}_{16}^{-1}. \quad (103)$$

(here $h\nu_{eff} \sim 10$ keV is the characteristic photon energy, ζ is the effective photoionization potential, $\sigma_{eff} \sim 10^{-24}$ cm² is the typical photoionization cross-section and $n_\gamma = L/(4\pi R^2 h\nu_{eff} c)$ is the photon number density). The photoionization to accretion time ratio at the effective Bondi radius is then

$$\frac{t_{pi}}{t_{accr}} \approx 0.07 f(u) \dot{M}_{16}^{-1}. \quad (104)$$

At wind velocities $v_w > 80$ km/s the bow shock stands at the classical Bondi radius R_B inside the effective Bondi radius R_B^* determined by (102). The cooling time of the shocked plasma at R_B expressed through the wind velocity v_w is:

$$t_{cool} \approx 4.7 \times 10^4 [\text{s}] \dot{M}_{16}^{-1} v_7^{0.2}. \quad (105)$$

The photoionization heating time in the post-shock region can also be expressed through the stellar wind velocity:

$$t_{pi} \approx 3.5 \times 10^4 [\text{s}] \dot{M}_{16}^{-1} v_7^{-4}. \quad (106)$$

A comparison of these two characteristic timescales implies that for low wind velocities radiative cooling becomes important and the source enters the regime of free-fall accretion with conservation of specific angular momentum.

Thus, for low wind velocities the plasma behind the shock cools down and starts to fall freely. As the cold plasma approaches the gravitating center, photoionization heating becomes important and rapidly heats up the plasma to $T_{max} \approx 5 \times 10^5$ K. Should this occur at a radius where $T_{max} < GM/(\mathcal{R}R)$, the plasma continues its free fall down to the magnetosphere, still with the temperature T_{max} , with the subsequent formation of a shock above the magnetosphere. However, if $T_{max} > GM/(\mathcal{R}R)$, settling accretion will work even for low wind velocities.

For high-wind stellar velocities $v_w \gtrsim 100$ km/s, the post-shock temperature is higher than T_{max} , photoionization is unimportant, and the settling accretion regime is established if the radiation cooling time is longer than the accretion time. From a comparison of these timescales, we find the critical accretion rate as a function of the wind velocity below which the settling accretion regime is possible:

$$\dot{M}_{16}^\ddagger \lesssim 0.12 v_7^{3.2}. \quad (107)$$

Here we stress the difference of the critical accretion rate \dot{M}^\ddagger and \dot{M}^\dagger , derived earlier. For $\dot{M} > \dot{M}^\ddagger$ the plasma rapidly cools down in the gravitational capture region and free-fall accretion begins (unless photoionization heats up the plasma above the adiabatic value at some radius), while at $\dot{M} > \dot{M}^\dagger \simeq 4 \times 10^{16}$ g/s, determined by (34) a free-fall gap appears immediately above the neutron star magnetosphere.

6.2 On the possibility of the propeller regime

The very slow rotation of the neutron stars in X-ray pulsars considered here (GX 1+4, GX 301-2, Vela X-1, SXP 1062, 4U 2204+56) with $\omega^*(R_A) < \omega_K(R_A)$ (see Table 1) makes it hard for these sources to enter the propeller regime where matter is ejected with parabolic velocities from the magnetosphere and the neutron star spins down.

Let us therefore start with estimating the important ratio of viscous tensions ($\sim B_t B_p$) to the gas pressure ($\sim B_p^2$) at the magnetospheric boundary. This ratio is proportional to B_t/B_p (see (73)) and is always much smaller than 1 (see Table 1), i.e. only large-scale convective motions where the characteristic hierarchy of eddies scales with radius can be established in the shell.

When $\omega^* > \omega_K(R_A)$, a centrifugal barrier is formed and accretion stops (the propeller regime). In that case the maximum possible braking torque is $\sim -\mu^2/R_A^3$ due to the strong coupling between the plasma and the magnetic field. Note that in the propeller state, interaction of the plasma with the magnetic field is by strong coupling, i.e. the toroidal magnetic field component B_t is comparable to the poloidal one B_p . It can not be excluded that a hot iso-angular-momentum envelope could exist in this case as well, which would then remove angular momentum from the rotating magnetosphere. If the characteristic cooling time of the gas in the envelope is short in comparison to the falling time of matter, the shell disappears and one can expect the formation of a ‘storing’ thin Keplerian disc around the neutron star magnetosphere [74]. There is no accretion of matter through such a disc. It only serves to remove angular momentum from the magnetosphere.

6.3 Effects of the hot shell on the X-ray energy and power spectrum

The spectra of X-ray pulsars are dominated by emission generated in the accretion column. The hot optically thin shell produces its own thermal emission, but even if all gravitational energy were released in the shell, the ratio of the X-ray luminosity from the shell to that of the accretion column would be about the ratio of the magnetospheric radius to that of the neutron star, i.e. one percent or less. In reality, the luminosity from the shell is much smaller. The shell should scatter X-ray radiation from the accretion column, but for this effect to be substantial, the Comptonization parameter y must be of the order of one. The Thomson depth in the shell is, however, very small. Indeed, from the mass continuity equation and (31) for the Alfvén radius and (33) for the factor $f(u)$, we get:

$$\tau_T = \int_{R_A}^{R_B} n_e(R) \sigma_T dR \approx 3.2 \times 10^{-3} \dot{M}_{16}^{8/11} \mu_{30}^{-2/11}.$$

Therefore, for the characteristic temperatures near the magnetosphere (see [(4)]) the parameter y is

$$y = \frac{4kT}{m_e c^2} \tau_T \approx 2.4 \times 10^{-3}.$$

This means that the X-ray spectrum, formed in the region of energy conversion close to the surface of the neutron star is not expected to be significantly altered by scattering in the hot shell.

Large-scale convective motions in the shell introduce an intrinsic time-scale of the order of the free-fall time that could give rise to features (e.g. QPOs) in the power spectrum of variability. QPOs were reported in some X-ray pulsars (see [75] and references therein). However, the expected frequencies of any QPOs arising in our model would be of the order of mHz, much higher than those reported.

A stronger effect could be the appearance of a dynamical instability in the shell due to increased Compton cooling and hence increased mass accretion rate through the shell. This may lead to a complete collapse of the shell triggering an X-ray outburst with duration similar to the free-fall time scale of the shell (~ 1000 s). Such transient behaviour is observed in the supergiant fast X-ray transients (SFXTs) see [76].) The possible development of such a scenario depends on the specific parameters of the shell and needs to be further investigated.

6.4 Can accretion discs (prograde or retrograde) be present in these pulsars?

Our analysis of the sample of pulsars in Section 5 suggested that in a convective shell an iso-angular-momentum distribution is the most plausible. Therefore, we shall below consider only this case, i.e. using

the rotation law $\omega \sim R^{-2}$. As follows from (61), at $\dot{\omega}^* = 0$ the equilibrium angular frequency of the neutron star is

$$\omega_{eq}^* = \omega_B \frac{1}{1 - z/Z} \left(\frac{R_B}{R_A} \right)^2. \quad (108)$$

We stress that such an equilibrium in our model is possible only when a shell is present. At high accretion rates $\dot{M} > \dot{M}_* \simeq 4 \times 10^{16}$ g/s accretion proceeds in the free-fall regime (with no shell present).

The equilibrium period for an X-ray pulsar in the quasi-spherical settling accretion regime can be derived using the formula (71): $P_{eq} \simeq 1300[\text{s}] \mu_{30}^{12/11} (P_b/10\text{d}) \dot{M}_{16}^{-4/11} v_8^4$.

For standard disc accretion, the equilibrium period is

$$P_{eq,d} \approx 7[\text{s}] \mu_{30}^{6/7} \dot{M}_{16}^{-3/7}, \quad (109)$$

and the long periods observed in some X-ray pulsars can thus, if a disc is present, be explained only assuming a very high magnetic field of the neutron star. Retrograde accretion discs are also discussed in the literature (see e.g. [29] and references therein). Torque reversals produced by temporary forming retrograde discs can in principle lead to very long periods for X-ray pulsars even with standard magnetic fields. Such retrograde discs could be formed as a result of inhomogeneities in the captured stellar wind [8, 9]. The scenario could, in principle, work for pulsars at high accretion rate, too high for a hot envelope to form.

In the case of GX 1+4, however, it is highly unlikely to observe a retrograde disk on a time scale much longer than the orbital period (see a more detailed discussion of this issue in [32]). For both GX 301-2 and Vela X-1, the observed positive torque-luminosity correlation (see Figs. 3 and 4) also rules out a retrograde disc in any of these systems.

To conclude this discussion section, we should mention that in reality, all pulsars (including those considered here) demonstrate a complex quasi-stationary behaviour with dips, outbursts, etc. These considerations are beyond the scope of this paper and definitely deserve further observational and theoretical studies.

7 Conclusions

In [14] we presented a theoretical model for quasi-spherical subsonic accretion onto slowly rotating magnetized neutron stars. In this model the accreting matter is gravitationally captured from the stellar wind of the optical companion and subsonically settles down onto the rotating magnetosphere forming an extended quasi-static shell. This shell mediates the angular momentum removal from the rotating neutron star magnetosphere by large-scale convective motions. Depending on the angular velocity of the rotating matter close to the magnetospheric boundary this type of accretion can cause the neutron star to either spin up or spin down.

A detailed analysis and comparison with observations of the two X-ray pulsars GX 301-2 and Vela X-1, both demonstrating positive torque-luminosity correlations near the equilibrium neutron star spin period, shows that the convective motions are most likely strongly anisotropic, and the rotational velocities in the shell $\omega \sim R^{-2}$ have a near iso-angular-momentum distribution. We note that a statistical analysis of long-period X-ray pulsars with Be-components in SMC by [33] also favored the rotation law $\omega \sim R^{-2}$.

The accretion rate through the shell is determined by the ability of the plasma to enter the magnetosphere. The settling regime of accretion which allows angular momentum removal from the neutron star magnetosphere can be realized for moderate accretion rates $\dot{M} < \dot{M}_* \simeq 4 \times 10^{16}$ g/s. At higher accretion rates a free-fall gap above the neutron star magnetosphere appears due to rapid Compton cooling, and accretion becomes highly non-stationary.

From observations of the spin-up/spin-down rates (the angular rotation frequency derivative $\dot{\omega}^*$, or $\partial\dot{\omega}^*/\partial\dot{M}$ near the torque reversal) of slowly rotating equilibrium X-ray pulsars with known orbital periods it is possible to determine the main dimensionless parameters of the model, as well as to estimate the magnetic field of the neutron star. Such an analysis revealed a good agreement between magnetic field estimates obtained using our model and those derived from cyclotron line measurements for the pulsars GX 301-2 and Vela X-1.

Using measurements of the spin period and the orbital period together with an estimate of the neutron star magnetic field μ , our model furthermore offers a possibility to estimate the stellar wind velocity of the companion, without the need for complicated spectroscopic measurements.

For non-equilibrium pulsars there is a maximum possible spin-down rate, depending on the spin period P^* , the orbital period P_b , the neutron star magnetic field μ and the wind velocity v_w . For such pulsars it is possible to estimate a lower limit on the neutron star magnetic field using the observed spin-down rate and X-ray luminosity. For the pulsars GX 1+4, SXP 1062, 4U 2206+54 investigated here, our estimates are all in agreement with standard field values and observed cyclotron line measurements.

In our model for quasi-spherical subsonic accretion, long-term spin-up/spin-down as observed in some X-ray pulsars can be quantitatively explained by a change in the mean mass accretion rate onto the neutron star (and the corresponding mean X-ray luminosity). Clearly, these changes are related to the stellar wind properties.

The model also predicts the specific behaviour of the variations in $\delta\dot{\omega}^*$, observed on top of a steady spin-up or spin-down, as a function of mass accretion rate fluctuations $\delta\dot{M}$. There is a critical accretion rate \dot{M}_{cr} below which an anti-correlation of $\delta\dot{\omega}^*$ with $\delta\dot{M}$ should occur (the case of GX 1+4 at the steady spin-down state currently observed), and above which $\delta\dot{\omega}^*$ should correlate with $\delta\dot{M}$ fluctuations (the case of Vela X-1, GX 301-2, and GX 1+4 in the steady spin-up state). The model explains quantitatively the relative amplitude and the sign of the observed frequency fluctuations in GX 1+4.

A The structure of a quasi-spherical rotating shell with accretion

A.1 Basic equations

Let us first write down the Navier-Stokes equations in spherical coordinates R, θ, ϕ . Due to the huge Reynolds numbers in the shell ($\sim 10^{15} - 10^{16}$ for a typical accretion rate of 10^{17} g/s and magnetospheric radius $\sim 10^8$ cm), there must be strong turbulence. In this case the Navier-Stokes equations are usually called the Reynolds equations. In the general case, the turbulent viscosity may depend on the coordinates, so the equations take the form:

1. Mass continuity equation:

$$\frac{\partial \rho}{\partial t} + \frac{1}{R^2} \frac{\partial}{\partial R} (R^2 \rho u_r) + \frac{1}{R \sin \theta} \frac{\partial}{\partial \theta} (\sin \theta \rho u_\theta) + \frac{1}{R \sin \theta} \frac{\partial \rho u_\phi}{\partial \phi} = 0. \quad (\text{A.1})$$

2. The R -component of the momentum equation:

$$\frac{\partial u_r}{\partial t} + u_r \frac{\partial u_r}{\partial R} + \frac{u_\theta}{R} \frac{\partial u_r}{\partial \theta} + \frac{u_\phi}{R \sin \theta} \frac{\partial u_r}{\partial \phi} - \frac{u_\phi^2 + u_\theta^2}{R} = -\frac{GM}{R^2} + N_R \quad (\text{A.2})$$

3. The θ -component of the momentum equation:

$$\frac{\partial u_\theta}{\partial t} + u_r \frac{\partial u_\theta}{\partial R} + \frac{u_\theta}{R} \frac{\partial u_\theta}{\partial \theta} + \frac{u_\phi}{R \sin \theta} \frac{\partial u_\theta}{\partial \phi} + \frac{u_r u_\theta - u_\phi^2 \cot \theta}{R} = N_\theta \quad (\text{A.3})$$

4. The ϕ -component of the momentum equation:

$$\frac{\partial u_\phi}{\partial t} + u_r \frac{\partial u_\phi}{\partial R} + \frac{u_\theta}{R} \frac{\partial u_\phi}{\partial \theta} + \frac{u_\phi}{R \sin \theta} \frac{\partial u_\phi}{\partial \phi} + \frac{u_r u_\phi + u_\phi u_\theta \cot \theta}{R} = N_\phi \quad (\text{A.4})$$

Here the force components (including viscous force and gas pressure gradients) read:

$$\rho N_R = \frac{1}{R^2} \frac{\partial}{\partial R} (R^2 W_{RR}) + \frac{1}{\sin \theta R} \frac{\partial}{\partial \theta} (W_{R\theta} \sin \theta) + \frac{1}{\sin \theta R} \frac{\partial}{\partial \phi} W_{R\phi} - \frac{W_{\theta\theta}}{R} - \frac{W_{\phi\phi}}{R} \quad (\text{A.5})$$

$$\rho N_\theta = \frac{1}{R^2} \frac{\partial}{\partial R} (R^2 W_{\theta R}) + \frac{1}{\sin \theta R} \frac{\partial}{\partial \theta} (W_{\theta\theta} \sin \theta) + \frac{1}{\sin \theta R} \frac{\partial}{\partial \phi} W_{\theta\phi} - \cot \theta \frac{W_{\theta\theta}}{R} \quad (\text{A.6})$$

$$\rho N_\phi = \frac{1}{R^3} \frac{\partial}{\partial R} (R^3 W_{\phi R}) + \frac{1}{\sin \theta R} \frac{\partial}{\partial \theta} (W_{\phi\theta} \sin \theta) + \frac{1}{\sin \theta R} \frac{\partial}{\partial \phi} W_{\phi\phi} \quad (\text{A.7})$$

The components of the stress tensor include a contribution from both the gas pressure P_g (assumed to be isotropic) and the turbulent pressure P^t (generally anisotropic). In their definition we shall follow the classical treatment by Landau and Lifshitz [77] but with the inclusion of anisotropic turbulent pressure:

$$W_{RR} = -P_g - P_{RR}^t + 2\rho\nu_t \frac{\partial u_r}{\partial R} - \frac{2}{3}\rho\nu_t \text{div} \mathbf{u} \quad (\text{A.8})$$

$$W_{\theta\theta} = -P_g - P_{\theta\theta}^t + 2\rho\nu_t \left(\frac{1}{R} \frac{\partial u_\theta}{\partial \theta} + \frac{u_r}{R} \right) - \frac{2}{3}\rho\nu_t \text{div} \mathbf{u} \quad (\text{A.9})$$

$$W_{\phi\phi} = -P_g - P_{\phi\phi}^t + 2\rho\nu_t \left(\frac{1}{R \sin \theta} \frac{\partial u_\phi}{\partial \phi} + \frac{u_r}{R} + \frac{u_\theta \cot \theta}{R} \right) - \frac{2}{3}\rho\nu_t \text{div} \mathbf{u} \quad (\text{A.10})$$

$$W_{R\theta} = \rho\nu_t \left(\frac{1}{R} \frac{\partial u_r}{\partial \theta} + \frac{\partial u_\theta}{\partial R} - \frac{u_\theta}{R} \right) \quad (\text{A.11})$$

$$W_{\theta\phi} = \rho\nu_t \left(\frac{1}{R \sin \theta} \frac{\partial u_\theta}{\partial \phi} + \frac{1}{R} \frac{\partial u_\phi}{\partial \theta} - \frac{u_\phi \cot \theta}{R} \right) \quad (\text{A.12})$$

$$W_{R\phi} = \rho\nu_t \left(\frac{1}{R \sin \theta} \frac{\partial u_r}{\partial \phi} + \frac{\partial u_\phi}{\partial R} - \frac{u_\phi}{R} \right) \quad (\text{A.13})$$

In our problem the anisotropy of the turbulence is such that $P_{RR}^t = P_{\parallel}^t$, $P_{\theta\theta}^t = P_{\phi\phi}^t = P_{\perp}^t$. The turbulent pressure components can be expressed through turbulent Mach numbers and will be given in Appendix E.

$\text{div} \mathbf{u}$ in spherical coordinates is:

$$\text{div} \mathbf{u} = \frac{1}{R^2} \frac{\partial}{\partial R} (R^2 u_r) + \frac{1}{R \sin \theta} \frac{\partial}{\partial \theta} (\sin \theta u_\theta) + \frac{1}{R \sin \theta} \frac{\partial u_\phi}{\partial \phi}. \quad (\text{A.14})$$

A.2 Symmetries of the problem

We shall consider axially-symmetric ($\frac{\partial}{\partial \phi} = 0$), stationary ($\frac{\partial}{\partial t} = 0$), and only radial accretion ($u_\theta = 0$). Under these conditions, from the continuity equation (A.1) we obtain:

$$\dot{M} = 4\pi R^2 \rho u_R = \text{const}. \quad (\text{A.15})$$

The constant here is determined from the condition of plasma leakage through the magnetosphere.

Let us rewrite the Reynolds equations under the above assumptions. The R -component of the momentum (A.2) equation becomes:

$$\rho \left(u_R \frac{\partial u_R}{\partial R} - \frac{u_\phi^2}{R} \right) = -\rho \frac{GM}{R^2} + \frac{1}{R^2} \frac{\partial}{\partial R} (R^2 W_{RR}) + \frac{1}{\sin \theta R} \frac{\partial}{\partial \theta} (W_{R\theta} \sin \theta) - \frac{W_{\theta\theta}}{R} - \frac{W_{\phi\phi}}{R} \quad (\text{A.16})$$

The θ -component of the momentum equation:

$$-\rho \frac{u_\phi^2 \cot \theta}{R} = \frac{1}{R^2} \frac{\partial}{\partial R} (R^2 W_{\theta R}) + \frac{1}{\sin \theta R} \frac{\partial}{\partial \theta} (W_{\theta\theta} \sin \theta) - \cot \theta \frac{W_{\theta\theta}}{R} \quad (\text{A.17})$$

The ϕ -component of the momentum equation:

$$\rho \left(u_R \frac{\partial u_\phi}{\partial R} + \frac{u_R u_\phi}{R} \right) = \frac{1}{R^3} \frac{\partial}{\partial R} (R^3 W_{\phi R}) + \frac{1}{\sin \theta R} \frac{\partial}{\partial \theta} (W_{\phi\theta} \sin \theta) \quad (\text{A.18})$$

The components of the stress tensor with anisotropic turbulence take the form:

$$W_{RR} = -P_g - P_{\parallel}^t - \frac{4}{3}\rho\nu_t \left(\frac{u_r}{R} - \frac{\partial u_r}{\partial R} \right) \quad (\text{A.19})$$

$$W_{\theta\theta} = -P_g - P_{\perp}^t + \frac{2}{3}\rho\nu_t \left(\frac{u_r}{R} - \frac{\partial u_r}{\partial R} \right) \quad (\text{A.20})$$

$$W_{\phi\phi} = -P_g - P_{\perp}^t + \frac{2}{3}\rho\nu_t \left(\frac{u_r}{R} - \frac{\partial u_r}{\partial R} \right) \quad (\text{A.21})$$

$$W_{R\theta} = \rho\nu_t \frac{1}{R} \frac{\partial u_r}{\partial \theta} \quad (\text{A.22})$$

$$W_{\theta\phi} = \rho\nu_t \left(\frac{1}{R} \frac{\partial u_\phi}{\partial \theta} - \frac{u_\phi \cot \theta}{R} \right) \quad (\text{A.23})$$

$$W_{R\phi} = \rho\nu_t \left(\frac{\partial u_\phi}{\partial R} - \frac{u_\phi}{R} \right) \quad (\text{A.24})$$

The main problem in describing gas dynamic flows with turbulence is in finding the kinematic viscosity parameter ν_t . As is well known, in the case of laminar flows the viscosity parameter ν is dependent only on the properties of the medium (liquid or gas). When turbulence is present, however, this coefficient is determined also by the macroscopic properties of the flow itself. There are some empirical relations which in principle can be verified experimentally. Most often the so called turbulent mixing length l_t is introduced. Furthermore L. Prandtl in his works introduced for plane-parallel shear flows (along the x-axis to be specific) the relation between the turbulent mixing length l_t , the velocity of the turbulent flow u_t and the characteristic amount of shear in the direction perpendicular to the average flow (z):

$$\nu_t = C_0 l_t \left| \frac{du}{dz} \right| \quad (\text{A.25})$$

where $C_0 \sim 1$ is a universal dimensionless constant, the exact numerical value of which should be determined from a theory that currently does not exist. In this way, the dependence of the turbulent stresses on the shear value becomes quadratic:

$$W_{zx} = \rho C_0 \left(\frac{du}{dz} \right)^2,$$

and a non-linearity is formed which in the general case makes the problem a lot more difficult.

First, we consider the general Prandtl law for turbulent viscosity in the case of an axis-symmetric flow. In the case of strong anisotropy there is one more empirical law for describing the turbulent viscosity, the Wasiutyński-law (see below), which is not reduced to the Prandtl law in the case of isotropic turbulence. This more general case for anisotropic turbulence will be discussed separately in Appendix C.

B Structure of the shell in the case of turbulent viscosity according to the Prandtl law

B.1 The empirical Prandtl law for axisymmetric flows with turbulent viscosity

. We consider an axisymmetric flow with a very large Reynolds number. By generalizing the Prandtl law for the turbulent velocity obtained for plane parallel flows, the turbulent velocity scales as $u_t \sim l_t R (\partial\omega/\partial R)$. From the similarity laws of gas-dynamics we assume $l_t \sim R$, so

$$u_t = C_1 R^2 \left| \frac{\partial\omega}{\partial R} \right|. \quad (\text{B.1})$$

We note that in our case the turbulent velocity is determined by convection, and thus $u_t \lesssim 0.5 u_{ff}$ (see Appendix D). This implies that the constant C_1 scales as

$$C_1 \sim u_t / \langle u_\phi \rangle, \quad (\text{B.2})$$

and can be very large since $\langle u_\phi \rangle \ll u_t$.

The turbulent viscosity coefficient thus reads:

$$\nu_t = \langle u_t l_t \rangle = C_2 C_1 R^3 \left| \frac{\partial\omega}{\partial R} \right| \quad (\text{B.3})$$

Here $C_2 \approx 1/3$ is a numerical factor originating from statistical averaging. Below we shall combine C_1 and C_2 into the new coefficient $C = C_1 C_2$, which can be much larger than unity.

For such a viscosity prescription the turbulent stresses $W_{R\phi}$ are equal to

$$W_{R\phi} = \rho \nu_t R \frac{\partial \omega}{\partial R} = \rho C R^4 \left(\frac{\partial \omega}{\partial R} \right)^2. \quad (\text{B.4})$$

B.2 The angular momentum transport equation

A similar problem (that of a rotating sphere in a viscous fluid) was solved in Landau and Lifshitz [77]. They showed that the variables here become separated and $u_\phi(R, \theta) = u_\phi(R) \sin \theta$. Note that the angular velocity $\omega(R) = u_\phi(R)/R$ is independent of the polar angle θ . Our problem is different from that of the sphere in a viscous fluid in several respects: 1) there is a force of gravity present, 2) the turbulent viscosity varies with R and can in principle depend on θ , and 3) there is radial motion of matter (accretion). These differences lead, as will be shown below, to the radial dependence $u_\phi(R) \propto R^{-1/2}$. (We recall that for a rotating sphere in a viscous fluid $u_\phi \propto R^{-2}$).

Let us start with solving (A.18). First, we note that for $u_\phi(\theta) \sim \sin \theta$, according to (A.23), $W_{\theta\phi} = 0$. Further, making use of the continuity equation (E.8) and the definition of angular velocity, we rewrite (A.18) in the form of angular momentum transfer by viscous forces:

$$\sin \theta \frac{\dot{M}}{R} \frac{\partial}{\partial R} \omega R^2 = \frac{4\pi}{R} \frac{\partial}{\partial R} R^3 W_{R\phi}. \quad (\text{B.5})$$

We rewrite equation (A.24) using the derivative of the angular velocity:

$$W_{R\phi} = \rho \nu_t R \frac{\partial \omega}{\partial R} \sin \theta. \quad (\text{B.6})$$

Substituting this expression into (B.5) and integrating over R , we get

$$\dot{M} \omega R^2 = 4\pi \rho \nu_t R^4 \frac{\partial \omega}{\partial R} + D, \quad (\text{B.7})$$

where D is an integration constant. This equation for angular momentum transport by turbulent viscosity is similar to that of disc accretion [2], but different due to spherical symmetry of our problem.

The left part of (B.7) is simply advection of specific angular momentum averaged over the sphere ($1/2 \int_0^\pi \omega R^2 \sin^2 \theta \sin \theta d\theta = 1/3 \omega R^2$) by the average motion toward the gravitational center (accretion). \dot{M} is negative as well as $\frac{\partial \omega}{\partial R}$. The first term on the right describes transport of angular momentum outwards by turbulent viscous forces.

The constant D is determined from the equation

$$D = \left(\frac{K_1}{\zeta} \right) K_2 \frac{\mu^2}{R_A^3} \frac{\omega_m - \omega^*}{\omega_K(R_A)} \quad (\text{B.8})$$

(see (52) in the text). We consider accretion onto a magnetized neutron star. When $D < 0$, the advection term in the left part of (B.7) dominates over viscous angular momentum transfer outwards. Oppositely, when $D > 0$, the viscous term in the right part of (B.7) dominates. In the case of $\dot{M} = 0$ (no plasma enters the magnetosphere), there is only angular momentum transport outwards by viscous forces.

Now let us rewrite (B.8) in the form

$$D = \left(\frac{K_1}{\zeta} \right) K_2 \frac{\mu^2}{R_A^6} R_A^3 \frac{\omega_m - \omega^*}{\omega_K(R_A)} \quad (\text{B.9})$$

and use the pressure balance condition

$$P(R_A) = P_g(R_A)(1 + \gamma m_i^2) = \frac{B^2(R_A)}{8\pi} = \frac{K_2}{2\pi} \frac{\mu^2}{R_A^6}. \quad (\text{B.10})$$

Using the mass continuity equation in the form

$$|\dot{M}| = 4\pi R^2 \rho f(u) \sqrt{GM/R},$$

and the expression for the gas pressure (8), we write the integration constant $D/|\dot{M}|$ in the form

$$\frac{D}{|\dot{M}|} = \left(\frac{K_1}{\zeta} \right) \frac{(\gamma - 1)}{\gamma} \psi(\gamma, m_t) \frac{(\omega_m - \omega^*) R_A^2}{2\sqrt{2}f(u)} (1 + \gamma m_t^2). \quad (\text{B.11})$$

Let us consider the case when the neutron star rotates close to equilibrium $\dot{\omega}^* = 0$. In this case according to (59)

$$\omega_m - \omega^* = -\frac{z}{Z} \omega^*, \quad (\text{B.12})$$

and thus using definition of Z [(57)], we obtain:

$$\frac{D}{|\dot{M}|} = -z R_A^2 \omega^*. \quad (\text{B.13})$$

We would like to stress that the value of the constant D is fully determined by the dimensionless specific angular momentum of matter at the Alfvén radius z .

B.3 The angular rotation law inside the shell

Let us now use (B.7) to find the rotation law $\omega(R)$. At large distances $R \gg R_A$ (we would like to remind the reader that R_A is the bottom radius of the shell), the constant D is small relative to the other terms, so we can set $D \approx 0$. Thus, to obtain the rotation law we shall neglect this constant in the right part of (B.7). Next, we substitute (B.3) and make use of the solution for the density (which, as we shall show below, remains the same as in the hydrostatic solution)

$$\rho(R) = \rho(R_A) \left(\frac{R_A}{R} \right)^{3/2} \quad (\text{B.14})$$

in equation (B.7) to obtain:

$$\left| \dot{M} \right| \omega R^2 = 4\pi \rho(R_A) \left(\frac{R_A}{R} \right)^{3/2} C R^7 \left(\frac{\partial \omega}{\partial R} \right)^2. \quad (\text{B.15})$$

After integrating this equation, we find

$$2\omega^{1/2} = \pm \frac{4}{3} \frac{K^{1/2}}{R^{3/4}} + D_1, \quad (\text{B.16})$$

where

$$K = \frac{|\dot{M}|}{4\pi \rho(R_A) C R_A^{3/2}} \quad (\text{B.17})$$

and D_1 is some integration constant. In (B.16) we use only the positive solution (the minus sign with constant $D_1 > 0$ would correspond to a solution with the angular velocity growing outwards, which is possible if the pulsar has a very long spin period, i.e. almost does not rotate at all). If $D_1 \neq 0$, at large $R \gg R_A$ (in the zone close to the bow shock) the solid body rotation law would lead to $\omega \rightarrow \text{const} \approx \omega_B$. (However, we remind the reader that our discussion is not applicable close to the bow shock region.) At small distances from the Alfvénic surface the effect of this constant is small and we shall neglect it in the calculations below. Then we find

$$\omega(R) = \frac{4}{9} \frac{|\dot{M}|}{4\pi \rho(R_A) C R_A^3} \left(\frac{R_A}{R} \right)^{3/2} \quad (\text{B.18})$$

i.e. the quasi-Keplerian law $\omega(R) = \omega_m (R_A/R)^{3/2}$. The value ω_m in the solution given by (B.18) is obtained after substituting \dot{M} from the continuity equation at $R = R_A$ into (B.18):

$$\omega_m \equiv \tilde{\omega} \omega(R_A) = \frac{4}{9} \tilde{\omega} \frac{|u_r(R_A)|}{C R_A}. \quad (\text{B.19})$$

(Here we have introduced the correction factor $\tilde{\omega} > 1$ to account for the deviation of the exact solution from the Keplerian law close to R_A).

As $u_R(R_A)$ is smaller than the free-fall velocity, the above formula implies that $\omega_m < \omega_K(R_A)$, lower than the Keplerian angular frequency. For self-consistency the coefficient C in the Prandtl law is determined, according to (B.19), by the ratio of the radial velocity u_R to the rotational velocity of matter u_ϕ :

$$C = \frac{4}{9} \tilde{\omega} \frac{|u_r(R_A)|}{\omega_m R_A} = \frac{4}{9} \tilde{\omega} \frac{|u_r(R_A)|}{u_\phi(R_A)}. \quad (\text{B.20})$$

We note that this ratio is independent of the radius R and is actually constant across the shell. Indeed, the radial dependence of the velocity u_R follows from the continuity equation with account for the density distribution (B.14)

$$u_r(R) = u_r(R_A) \left(\frac{R_A}{R} \right)^{1/2}. \quad (\text{B.21})$$

For a quasi-Keplerian law $u_\phi(R) \sim 1/R^{1/2}$, so the ratio u_r/u_ϕ is constant.

Finally, the angular frequency of the rotation of the shell near the magnetosphere ω_m is related to the angular frequency of the motion of matter near the bow-shock as

$$\omega_m = \tilde{\omega} \omega_B \left(\frac{R_B}{R_A} \right)^{3/2}. \quad (\text{B.22})$$

In fact, when approaching R_A , the integration constant D (which we neglected at large distances $R \gg R_A$) should be taken into account. The rotational law will thus somewhat differ from a quasi-Keplerian close to the magnetosphere.

We stress the principal difference between this regime of accretion and disc accretion. For disc accretion the radial velocity is much smaller than the turbulent velocity, and the tangential velocity is almost Keplerian and is much larger than the turbulent velocity. The radial velocity in the quasi-spherical case is not determined by the rate of the angular momentum removal. It is determined only by the "permeability" of the neutron star magnetosphere for infalling matter. In our case we assume that the radial velocity is of the order of the velocity of convective motions in the shell. The tangential velocity for the obtained quasi-Keplerian law is much smaller than the velocity of the convective motions. Note also that in the case of disc accretion the turbulence can be parametrized by only one dimensionless parameter $\alpha \approx u_t^2/u_s^2$ with $0 < \alpha < 1$ [2]. The matter in an accretion disc rotates differentially with a supersonic (almost Keplerian) velocity, while in our case the shell rotates differentially with a clearly subsonic velocity at any radius, and the turbulence in the shell is essentially subsonic. Also, our case with an extended shell is of course strongly different from the regime of freely falling matter with a standing shock above the magnetosphere [17].

B.4 The case without accretion

Now let us consider the case where the plasma can not enter the magnetosphere and no accretion onto the neutron star occurs. This case is similar to the subsonic propeller regime considered by Davies and Pringle [11]. (B.7) then takes the form:

$$0 = 4\pi\rho\nu_t R^4 \frac{\partial\omega}{\partial R} + D. \quad (\text{B.23})$$

(Remember that the constant D is determined by the spin-down rate of the neutron star, $D = I\dot{\omega}^* < 0$). Solving this equation as above, we find for the rotation law without accretion:

$$\omega(R) = \omega_m \left(\frac{R_A}{R} \right)^{7/4}, \quad (\text{B.24})$$

where

$$\omega_m = \frac{I|\dot{\omega}^*|}{7\pi\rho(R_A)\nu_t(R_A)R_A^3}. \quad (\text{B.25})$$

From (B.3) we find

$$\nu_t(R_A) = \frac{7}{4} C \omega_m R_A^2, \quad (\text{B.26})$$

and thus for ω_m we obtain:

$$\omega_m = \frac{2}{7} \left(\frac{I|\dot{\omega}^*|}{\pi C \rho (R_A) R_A^5} \right)^{1/2}. \quad (\text{B.27})$$

However, ω_m is also related to the bow-shock region parameters as

$$\omega_m = \omega_B \left(\frac{R_B}{R_A} \right)^{7/4}, \quad (\text{B.28})$$

which can in principle be used to further study this case, which we shall not do here.

C Structure of the shell and angular rotation law in case of turbulent viscosity according to Wasiutyński

Prandtl's law for viscosity that was used above relates the scale and velocity of turbulent pulsations with the average angular velocity and is commonly used when the turbulence is generated by the shear itself. In our problem, the turbulence is initiated by large-scale convective motions in the gravitational field. Due to convection, strong anisotropic turbulent motions may appear (the radial dispersion of chaotic motions could be much larger than the dispersion in the tangential direction), and Prandtl's law may thus be inapplicable.

Anisotropic turbulence is much more complicated and remains poorly studied. As a first step, we may adopt the empirical law for $W_{R\phi}$ as suggested by Wasiutyński [78]:

$$W_{R\phi} = 2\rho(-\nu_t + \nu_r)\omega + \nu_r \rho R \frac{d\omega}{dR}, \quad (\text{C.1})$$

where the radial and tangential kinematic viscosity coefficients are

$$\nu_r = C_{\parallel} \langle |u_{\parallel}^t| \rangle R$$

$$\nu_t = C_{\perp} \langle |u_{\perp}^t| \rangle R$$

respectively. The dimensionless constants C_{\parallel} and C_{\perp} are of the order of one. In the isotropic case $\nu_r = \nu_t$, $W_{R\phi} \sim d\omega/dR$, and in the strongly anisotropic case $\nu_r \gg \nu_t$, $W_{R\phi} \sim d(\omega R^2)/dR$. Using these definitions, let us substitute (C.1) into (B.5), and after integration over R rewrite the latter in the form:

$$\omega R^2 \left(1 - \frac{2C_{\perp} \langle |u_{\perp}^t| \rangle}{|u_r|} \right) = C_{\parallel} \frac{\langle |u_{\parallel}^t| \rangle}{|u_r|} \frac{R d(\omega R^2)}{dR} - \frac{D}{|M|}. \quad (\text{C.2})$$

We note that due to self-similarity in the shell structure $u_{\parallel}^t \sim u_{\perp}^t \sim u_r \sim R^{-1/2}$, and thus the ratios $\langle |u_{\parallel}^t| \rangle / u_r$ and $\langle |u_{\perp}^t| \rangle / u_r$ are constant. In this case the obvious solution to the above equation reads:

$$\omega R^2 + \frac{D}{|M|} \frac{1}{1 - 2C_{\perp} \frac{\langle |u_{\perp}^t| \rangle}{|u_r|}} = \left[\omega_B R_B^2 + \frac{D}{|M|} \frac{1}{1 - 2C_{\perp} \frac{\langle |u_{\perp}^t| \rangle}{|u_r|}} \right] \left(\frac{R_B}{R} \right)^{\frac{|u_r|}{C_{\parallel} \langle |u_{\parallel}^t| \rangle}} \left(1 - 2C_{\perp} \frac{\langle |u_{\perp}^t| \rangle}{|u_r|} \right) \quad (\text{C.3})$$

(here the integration constant is defined as such that $\omega(R_B) = \omega_B$).

Now let us consider the equilibrium situation where $\dot{\omega}^* = 0$. In this case, as we remember,

$$\frac{D}{|M|} = -z\omega^* R_A^2, \quad \omega_m = (1 - z/Z)\omega^*.$$

First, let us consider the case of strongly anisotropic, almost radial turbulence where $\langle |u_{\perp}^t| \rangle = 0$. In this case, the specific angular momentum at the Alfvén radius is

$$\omega_m R_A^2 \left[1 + \frac{z}{1 - z/Z} \left(\left(\frac{R_B}{R_A} \right)^{\frac{|u_r|}{C_{\parallel} \langle |u_{\parallel}^t| \rangle}} - 1 \right) \right] = \omega_B R_B^2 \left(\frac{R_B}{R_A} \right)^{\frac{|u_r|}{C_{\parallel} \langle |u_{\parallel}^t| \rangle}}. \quad (\text{C.4})$$

From this we see that in the case of very weak accretion (or, in the limit, when there is no accretion through the magnetosphere at all), $|u_R| \ll C_{\parallel} \langle |u_{\parallel}^t| \rangle$, and an almost iso-angular-momentum distribution of rotational velocities in the shell is formed.

The next case is where the amount of anisotropy is such that $C_{\perp} \langle |u_{\perp}^t| \rangle / |u_r| = 1/2$. Then we have a strict iso-angular-momentum distribution in the shell: $\omega_m R_A^2 = \omega_B R_B^2$.

If the turbulence is fully isotropic $C_{\perp} \langle |u_{\perp}^t| \rangle = C_{\parallel} \langle |u_{\parallel}^t| \rangle = \tilde{C} \langle |u^t| \rangle$. Denoting $\epsilon = |u_r| / (\tilde{C} \langle |u^t| \rangle)$, we find:

$$\omega_m R_A^2 \left[1 + \left(\frac{z}{1 - z/Z} \right) \left(\frac{1}{2/\epsilon - 1} \right) \left(1 - \left(\frac{R_A}{R_B} \right)^{2-\epsilon} \right) \right] = \omega_B R_B^2 \left(\frac{R_A}{R_B} \right)^{2-\epsilon}. \quad (\text{C.5})$$

Note that if $\epsilon \rightarrow 0$ (and there is no accretion through the magnetosphere), $\omega_m \rightarrow \omega_B$, and we have solid-body rotation without accretion (cf. the first case above!). For $\epsilon = 3/2$, a near quasi-Keplerian angular rotation distribution may be established. We remind the reader that a similar quasi-Keplerian distribution was obtained in Appendix B above with the use of the Prandtl law for isotropic turbulent viscosity. In that case, this was the only solution. Here, in contrast, the quasi-Keplerian law is only one particular case of the general solution obtained using Wasiutyński's prescription for anisotropic turbulent viscosity.

As we have shown in the main text, a quasi-Keplerian rotation law is not favored by observations. We therefore conclude that the most likely velocity distribution in the shell is the near iso-angular-momentum one with anisotropic turbulence initiated by convection. Note that for thin accretion discs where the vertical height limits the scale of the turbulence, the Prandtl law for viscosity works very well [2].

D Corrections to the radial temperature gradient

Here we shall estimate how the radial temperature gradient differs from the adiabatic law due to the convective motions in the shell. By multiplying (56) by $(1/2)(\omega_m - \omega^*)$, we obtain the convective heating rate caused by interaction of the shell with the magnetosphere:

$$L_c = \frac{1}{2} Z \dot{M} R_A^2 (\omega_m - \omega^*)^2. \quad (\text{D.1})$$

Multiplying the same (56) with ω^* yields the rate of change of the mechanical energy of the neutron star

$$L_k = Z \dot{M} R_A^2 \omega^* (\omega_m - \omega^*). \quad (\text{D.2})$$

The total energy balance is then

$$L_t = L_c + L_k = \frac{1}{2} Z \dot{M} R_A^2 (\omega_m^2 - \omega^{*2}). \quad (\text{D.3})$$

Note that the obtained formula for L_c is similar to that describing energy release in the boundary layer of an accretion disc, see [79].

The convective energy flux is:

$$q_c = \frac{L_c}{4\pi R^2} = \frac{Z \dot{M} R_A^2 (\omega_m - \omega^*)^2}{8\pi R^2}. \quad (\text{D.4})$$

The convective energy flux can also be related to the entropy gradient as [80]):

$$q_c = -\rho \nu_c T \frac{dS}{dR}, \quad (\text{D.5})$$

where S is the specific entropy (per gram). Here ν_c is the radial turbulent heat conductivity

$$\nu_c = \langle u_c l_c \rangle = C_h u_c R, \quad (\text{D.6})$$

where the characteristic scale of convection $l_c \sim R$, the velocity of convective motions $u_c \sim c_s \sim R^{-1/2}$, and C_h is a numerical coefficient of the order of one. Thus

$$\nu_c = \nu_c(R_A) \left(\frac{R}{R_A} \right)^{1/2}. \quad (\text{D.7})$$

Next, we make use of the thermodynamic identity for the specific enthalpy H :

$$\frac{dH}{dR} = \frac{1}{\rho} \frac{dP_g}{dR} + T \frac{dS}{dR}. \quad (\text{D.8})$$

We remind the reader that the enthalpy can be written as

$$dH = c_p dT,$$

where

$$c_p = T \left(\frac{\partial S}{\partial T} \right)_p = \frac{\gamma}{\gamma - 1} \frac{\mathcal{R}}{\mu_m}$$

is the specific heat capacity at constant pressure. Expressing $T(dS/dR)$ from (D.5) and making use of the hydrostatic equation [(4)] written as

$$\frac{dP_g/\rho}{dR} = -\frac{\mathcal{R}}{\mu_m c_p} \frac{GM}{R^2} \psi(\gamma, m_t).$$

the thermodynamic identity (D.8) can be rewritten in the form

$$\frac{dT}{dR} = -\frac{1}{c_p} \left[\frac{GM}{R^2} \psi(\gamma, m_t) - \frac{Z u_r(R_A)}{2\nu_c(R_A)} \left(\frac{R_A}{R} \right) R_A^2 (\omega_m - \omega^*)^2 \right]. \quad (\text{D.9})$$

By definition the adiabatic temperature gradient is determined by the first term on the right hand side ($dT/dR)_{ad} = g/c_p$. Equation (D.9) can be integrated to find the actual dependence of the temperature on the radius in the convective shell:

$$T = \frac{1}{c_p} \left[\frac{GM}{R} \psi(\gamma, m_t) - \frac{Z u_r(R_A)}{2\nu_c(R_A)} R_A^3 (\omega_m - \omega^*)^2 \ln \left(\frac{R}{R_A} \right) \right]. \quad (\text{D.10})$$

Close to equilibrium ($I\dot{\omega}^* = 0$), we can use (B.12) and write

$$T = \frac{1}{c_p} \left[\frac{GM}{R} \psi(\gamma, m_t) - \frac{u_r(R_A)}{2C_h u_c(R_A)} \omega^{*2} R_A^2 \frac{z^2}{Z} \ln \left(\frac{R}{R_A} \right) \right]. \quad (\text{D.11})$$

This solution shows that in the whole region between R_A and R_B , for slowly rotating pulsars (i.e., in which $\omega_m \ll \omega_K(R_A)$), the temperature distribution is close to the adiabatic law with a temperature gradient close to the adiabatic one [(4)]:

$$T \approx \frac{\gamma - 1}{\gamma} \frac{GM}{\mathcal{R}R} \psi(\gamma, m_t). \quad (\text{D.12})$$

Here we have only taken into account energy release due to the frequency difference near the magnetosphere. In reality, there may be additional sources of energy in the shell (e.g. the heat release during magnetic reconnection and turbulence (see Appendix E), etc.).

E Dynamics of a stationary spherically-symmetric ideal gas flow

In this Appendix, we write down the gas-dynamic equations of a spherically symmetric ideal gas flow onto a Newtonian gravitating center. This problem was considered in the classical paper by Bondi ([18]) for an adiabatic accretion flow. Adiabatic gas outflows (stellar winds) were studied by Parker [81]. A thorough and comprehensible discussion of such flows can be found in the monograph by V. Beskin [82]. Here we focus on the role of the cooling/heating processes near the Alvenic surface, and also take into account the effects of turbulence and/or convection (anisotropy in general). As discussed in the main text, at low X-ray luminosities the quasi-static shell is capable of removing angular momentum from the rotating magnetosphere via convective motions. As the accretion rate exceeds some critical value, strong Compton cooling causes a free-fall gap to appear above the magnetosphere, and angular momentum cannot be transferred from the magnetosphere to the shell any more.

The equation of motion (A.16) in the absence of viscosity reads:

$$u_r \frac{du_r}{dR} = -\frac{1}{\rho} \frac{dP_g}{dR} - \frac{1}{\rho} \frac{dP_{\parallel}^t}{dR} - \frac{2(P_{\parallel}^t - P_{\perp}^t)}{\rho R} - \frac{GM}{R^2} \quad (\text{E.1})$$

Here $P_g = \rho c_s^2 / \gamma$ is the gas pressure, and P^t the pressure due to turbulent pulsations, which in general are anisotropic:

$$P_{\parallel}^t = \rho \langle u_{\parallel}^2 \rangle = \rho m_{\parallel}^2 c_s^2 = \gamma P_g m_{\parallel}^2 \quad (\text{E.2})$$

$$P_{\perp}^t = 2\rho \langle u_{\perp}^2 \rangle = 2\rho m_{\perp}^2 c_s^2 = 2\gamma P_g m_{\perp}^2 \quad (\text{E.3})$$

$\langle u_t^2 \rangle = \langle u_{\parallel}^2 \rangle + 2 \langle u_{\perp}^2 \rangle$ is the turbulent velocity dispersion, m_{\parallel}^2 and m_{\perp}^2 are the parallel and perpendicular turbulent Mach numbers squared).

From the first law of thermodynamics we have

$$\frac{dE}{dR} = \frac{P_g}{\rho} \frac{d\rho}{dR} + T \frac{dS}{dR}, \quad (\text{E.4})$$

where the specific internal energy (per gram) is

$$E = c_V T = \frac{c_s^2}{\gamma(\gamma - 1)}, \quad (\text{E.5})$$

and the heat capacity is

$$c_V = \frac{\mathcal{R}}{\mu_m} \frac{1}{\gamma - 1}. \quad (\text{E.6})$$

From the second law of thermodynamics, the specific entropy change can be written using the rate of the specific heat change dQ/dt [erg/s/g] as

$$T \frac{dS}{dR} = \frac{dQ}{dR} = \frac{dQ/dt}{u_r}. \quad (\text{E.7})$$

Using the mass continuity equation

$$\dot{M} = 4\pi R^2 \rho u_r, \quad (\text{E.8})$$

we find

$$\frac{1}{\rho} \frac{d\rho}{dR} = -\frac{2}{R} - \frac{1}{2u_r^2} \frac{du_r^2}{dR}. \quad (\text{E.9})$$

Using the relation $c_s^2 = \gamma \mathcal{R} T$, we finally obtain:

$$\frac{1}{c_s^2} \frac{dc_s^2}{dR} = (\gamma - 1) \left[-\frac{2}{R} - \frac{1}{2u_r^2} \frac{du_r^2}{dR} \right] + \frac{dQ/dt}{u_r c_V T}. \quad (\text{E.10})$$

Note that this equation can also be derived directly from the ideal gas equation of state written in the form

$$P_g = K e^{S/c_V} \rho^{\gamma}, \quad (\text{E.11})$$

where K is some constant.

Using (E.10), the gas pressure gradient can be rewritten in the form:

$$\frac{1}{P_g} \frac{dP_g}{dR} = \frac{c_s^2}{c_V u_r} \frac{dQ/dt}{T} + c_s^2 \left[-\frac{2}{R} - \frac{1}{2u_r^2} \frac{du_r^2}{dR} \right] \quad (\text{E.12})$$

Plugging (E.12) into the equation of motion finally yields:

$$\frac{1}{2} \frac{1}{u_r^2} \frac{du_r^2}{dR} = \left[c_s^2 (1 + \gamma m_{\parallel}^2) \left(\frac{2}{R} - \frac{dQ/dt}{c_V u_r T} \right) - 2c_s^2 \frac{(m_{\parallel}^2 - m_{\perp}^2)}{R} - \frac{GM}{R^2} \right] / \left[u_r^2 - c_s^2 (1 + \gamma m_{\parallel}^2) \right]. \quad (\text{E.13})$$

Note also that in the strongly anisotropic case where $m_{\parallel}^2 = m_t^2 \gg m_{\perp}^2$, the role of turbulence increases in comparison with the isotropic case where $m_{\parallel}^2 = m_{\perp}^2 = (1/3)m_t^2$.

We can also introduce the Mach number in the flow $\mathcal{M} \equiv u_r/c_s$. Then from (E.10) and (E.13) we derive the equation for the Mach number:

$$\left\{ \frac{[\mathcal{M}^2 - (1 + \gamma m_{\parallel}^2)]}{\mathcal{M}^2} \frac{d\mathcal{M}^2}{dR} = \frac{2[(\gamma-1)\mathcal{M}^2 - (\gamma+1)(m_{\parallel}^2 - m_{\perp}^2)]}{R} - \frac{[\mathcal{M}^2 + \gamma(1 + \gamma m_{\parallel}^2)]}{c_v T} \frac{dQ}{dR} - \frac{(\gamma+1)GM}{R^2 c_s^2} \right\}, \quad (\text{E.14})$$

where we have substituted $(dQ/dt) = u(dQ/dR)$. Equations (E.10), (E.13) and (E.14) can be used to solve the dynamics of the accretion flow for pairs of independent variables (u, c_s) , (u, \mathcal{M}) or (c_s, \mathcal{M}) . Here, however, we shall only consider the behaviour of the flux near the singular point. To this end, we can use (E.13).

(E.13) has a singular saddle point where the denominator vanishes:

$$u_r^2 = c_s^2(1 + \gamma m_{\parallel}^2). \quad (\text{E.15})$$

So must the numerator, from which we find the quadratic equation for the velocity at the singular point:

$$u_r^2 \frac{2}{R} \left(\frac{1 + (\gamma - 1)m_{\parallel}^2 + m_{\perp}^2}{1 + \gamma m_{\parallel}^2} \right) - u_r \left(\frac{dQ/dt}{c_v T} \right) - \frac{GM}{R^2} = 0. \quad (\text{E.16})$$

Remember that in the adiabatic case ($dQ/dt = 0$) without turbulence at the saddle point we have simply

$$u_r^2 = c_s^2 = \frac{GM}{2R}. \quad (\text{E.17})$$

We stress that the presence of turbulence increases the velocity at the singular point. For example, for $\gamma = 5/3$ we find for strong anisotropic turbulence $u^2 = c_s^2(1 + (5/3)m_{\parallel}^2)$; for the isotropic turbulence the correction is smaller: $u^2 = c_s^2(1 + (5/9)m_{\parallel}^2)$. The transition through the sound speed (the sonic point where $u^2 = c_s^2$) lies above the saddle point due to turbulence, and there is no singularity in the sonic point.

First let us determine the turbulence heating rate in the quasi-static shell $(dQ/dt)_t^+$:

$$\left(\frac{dQ}{dt} \right)_t^+ = \frac{1}{2} \frac{u_t^2}{t_t}, \quad (\text{E.18})$$

where the characteristic time of the turbulent heating is

$$t_t = \alpha_t \frac{R}{u_t} = \alpha_t \frac{R}{m_t c_s}, \quad (\text{E.19})$$

with α_t being a dimensionless constant characterizing the turbulent dissipation energy rate and the turbulent Mach number is $m_t^2 \equiv m_{\parallel}^2 + 2m_{\perp}^2$. The turbulent heating rate can thus be written as

$$\left(\frac{dQ}{dt} \right)_t^+ = \frac{c_s^3}{2\alpha_t R} m_t^3. \quad (\text{E.20})$$

In the case of Compton cooling we have

$$\left(\frac{dQ}{dt} \right)_C^- = -\frac{c_v(T - T_x)}{t_C}, \quad (\text{E.21})$$

where t_C is the Compton cooling time [(17)].

(E.16) can now be written in the form:

$$u_r^2 \frac{2}{R} \left(\frac{1 + (\gamma - 1)m_{\parallel}^2 + m_{\perp}^2}{1 + \gamma m_{\parallel}^2} \right) - u_r^2 \frac{c_s}{u_r} \frac{\gamma(\gamma - 1)m_t^3}{2\alpha_t R} + \frac{u_r(1 - T_x/T)}{\gamma t_C} - \frac{GM}{R^2} = 0. \quad (\text{E.22})$$

As we study the accretion problem, the sign of the velocity $u_r = dR/dt$ is negative, so below we shall write $u_r = -|u_r|$. Then for the absolute value of the velocity at the singular point where the sound speed is $c_s/|u_r| = -1/(1 + \gamma m_{\parallel}^2)^{1/2}$ we have the quadratic equation:

$$u_r^2 \frac{2}{R} \left(\frac{1 + (\gamma - 1)m_{\parallel}^2 + m_{\perp}^2}{1 + \gamma m_{\parallel}^2} \right) + u_r^2 \frac{1}{(1 + \gamma m_{\parallel}^2)^{1/2}} \frac{\gamma(\gamma - 1)m_t^3}{2\alpha_t R} - \frac{|u_r|(1 - T_x/T)}{\gamma t_C} - \frac{GM}{R^2} = 0. \quad (\text{E.23})$$

In this case, the solution to (E.16) reads:

$$|u_r| = \frac{R(1 - T_x/T)}{4\gamma t_C A} + \sqrt{\frac{2GM}{R}} \left[\frac{1}{4A} + \frac{R}{2GM} \frac{R^2(1 - T_x/T)^2}{16\gamma^2 t_C^2 A^2} \right]^{1/2}, \quad (\text{E.24})$$

where we have introduced the dimensionless factor

$$A = \frac{1 + (\gamma - 1)m_{\parallel}^2 + m_{\perp}^2}{1 + \gamma m_{\parallel}^2} + \frac{\gamma(\gamma - 1)(m_{\parallel}^2 + 2m_{\perp}^2)^{3/2}}{4\alpha_t(1 + \gamma m_{\parallel}^2)^{1/2}}. \quad (\text{E.25})$$

In the case of isotropic turbulence where $m_{\parallel} = m_{\perp} = 1/\sqrt{3}$, $m_t = 1$, for $\gamma = 5/3$ the factor $A \approx 1.23$, and in the case of strongly anisotropic turbulence where $m_{\parallel} = 1$, $m_{\perp} = 0$, $m_t = 1$, this factor is $A \approx 0.8$.

In units of the free-fall velocity the solution (E.24) reads:

$$f(u) = \frac{|u_r|}{u_{ff}} = \frac{(1 - T_x/T)}{4\gamma A} \left(\frac{t_{ff}}{t_C} \right) + \frac{1}{2} \left[\frac{1}{A} + \frac{(1 - T_x/T)^2}{4\gamma^2 A^2} \left(\frac{t_{ff}}{t_C} \right)^2 \right]^{1/2}. \quad (\text{E.26})$$

With Compton cooling present, the temperature changes exponentially:

$$T = T_x + (T_{cr} - T_x)e^{-t/t_C} \quad (\text{E.27})$$

see the main text). When cooling is slow, $t_{ff}/t_C \ll 1$, the critical point lies inside the Alfvén surface, i.e. no transition through the critical point occurs in the flow before it meets the magnetosphere, and in this case we expect settling accretion. If this point lies above the Alfvén surface, the velocity of the flow may become supersonic above the magnetosphere, and one may thus expect the formation of a shock. Both turbulence and rapid cooling shifts the location of the critical point upwards in the flow.

In the case of rapid cooling $t_{ff}/t_C \gg 1$, $T \rightarrow T_x$, so again $u_r/u_{ff} \approx 1/2$ (cf. (E.17) for an adiabatic flow), but the critical point now lies above the Alfvén surface, so a free-fall gap above the magnetosphere appears. The ratio $f(u) = |u_r|/u_{ff}$ reaches a maximum at $t_{ff}/t_C \approx 0.46$ (assuming a typical ratio $T_{cr}/T_x = 10$), and depending on the value of $A = 0.8 \div 1.23$ (anisotropic or isotropic turbulence) it equals to $f(u) = 0.5 - 0.6$.

Acknowledgements

The authors would like to thank Dr. V. Doroshenko (IAAT) for courtesly providing the torque-luminosity plots for GX 301-2 and Vela X-1, and Dr. V. Beskin and Dr. V. Suleimanov for discussions. NIS thanks the Max-Planck Institute for Astrophysics (Garching) for shown hospitality. The work by NIS, KAP and AYK is supported by RFBR grants 09-02-00032, 12-02-00186 and 10-02-00599. LH is supported by a grant from the Wenner-Gren foundations (Sweden).

References

- [1] Bildsten L et al *Astrophys. J. Suppl.* **113** 367(1997)
- [2] Shakura N I, Sunyaev R A *Astron. Astrophys.* **24** 337 (1973)
- [3] Pringle J E, Rees M J *Astron. Astrophys.* **21** 1 (1972)
- [4] Ghosh P, Lamb F K *Astrophys. J.* **234** 296 (1979)
- [5] Lovelace R V E, Romanova M M, Bisnovatyi-Kogan G S *Mon. Not. R. Astron. Soc.* **275** 244 (1995)
- [6] Kluźniak W, Rappaport S *Astrophys. J.* **671** 1990 (2007)
- [7] Fryxell B A, Taam R E *Astrophys. J.* **335** 862 (1988)
- [8] Ruffert M *Astron. Astrophys.* **317** 793 (1997)
- [9] Ruffert M *Astron. Astrophys.* **346** 861 (1999)

- [10] Burnard D J, Arons J, Lea S M *Astrophys. J.* **266** 175 (1983)
- [11] Davies R E, Pringle J E *Mon. Not. R. Astron. Soc.* **196** 209 (1981)
- [12] Illarionov A F, Kompaneets D A *Mon. Not. R. Astron. Soc.* **247** 219 (1990)
- [13] Bisnovaty-Kogan G S *Astron. Astrophys.* **245** 528 (1991)
- [14] Shakura N I, Postnov K A, Kochetkova A Yu, Hjalmarsdotter L *Mon. Not. R. Astron. Soc.* **420** 216 (2012)
- [15] Illarionov A F, Sunyaev R A *Astron. Astrophys.* **39** 185 (1975)
- [16] Elsner R F, Lamb F K *Astrophys. J.* **215** 897 (1977)
- [17] Arons J, Lea S M *Astrophys. J.* **207** 914 (1976)
- [18] Bondi H (*Mon. Not. R. Astron. Soc.*) **112** 195 (1952)
- [19] Kompaneets A S *ZhETP* **31** 876 (1956)
- [20] Weymann R *Phys. Fluids* **8** 2112 (1965)
- [21] Shakura N I, Postnov K A, Hjalmarsdotter L *Mon. Not. R. Astron. Soc.* **428** 670 (2013)
- [22] Doroshenko V, Santangelo A, Suleimanov V *Astron. Astrophys.* **529** 52 (2011)
- [23] Finger M et al <http://gammaray.nsstc.nasa.gov/gbm/science/pulsars/lightcurves/gx1p4.html>
- [24] Ikhsanov N R, Beskrovnaya N G *Astron. Rep.* **56** 589 (2012)
- [25] Lipunov V M *Astrophysics of Neutron Stars* (Berlin: Springer, 1992)
- [26] Chakrabarty D et al *Astrophys. J. Lett.* **481** L101 (1997)
- [27] Sunyaev R A in: *Physics and astrophysics of neutron stars and black holes* (Amsterdam: North Holland Publ., 1978) p. 697
- [28] Ho C et al *Mon. Not. R. Astron. Soc.* **238** 1447 (1989)
- [29] Nelson R W et al *Astrophys. J.* **488** L117 (1997)
- [30] Arons J, Lea S M *Astrophys. J.* **210** 792 (1976)
- [31] Hunt R *Mon. Not. R. Astron. Soc.* **154** 141 (1971)
- [32] González-Galán A et al *Astron. Astrophys.* **537** A66 (2012)
- [33] Chashkina A A, Popov S B *New Astron.* **17** 594 (2012)
- [34] Lue G-L et al *Mon. Not. R. Astron. Soc.* **424** 2265 (2012)
- [35] Lutovinov A, Tsygankov S, Chernyakova M *Mon. Not. R. Astron. Soc.* **423** 1978 (2012)
- [36] Marcu D M et al *Astrophys. J.* **742** L11 (2011)
- [37] Popov S B, Turolla R *Mon. Not. R. Astron. Soc.* **421** L127 (2012)
- [38] Fu L, Li X-D, *Astrophys. J.* **757** id171 (2012)
- [39] Koh D T et al *Astrophys. J.* **479** 933 (1997)
- [40] White N E et al *Astrophys. J.* **209** L119 (1976)
- [41] Kaper L, van der Meer A, Najjarro F *Astron. Astrophys.* **457** 595 (2006)
- [42] de Kool M, Anzer U *Mon. Not. R. Astron. Soc.* **262** 726 (1993)
- [43] Nagase F *Publ. Astron. Soc. Jap.* **41** 1 (1989)

- [44] Pravdo S H, Ghosh P *Astrophys. J.* **554** 383 (2001)
- [45] La Barbera A et al *Astron. Astrophys.* **438** 617 (2005)
- [46] Kreykenbohm I et al *Astron. Astrophys.* **427** 975 (2004)
- [47] Doroshenko V et al *Astron. Astrophys.* **515** A10 (2010)
- [48] Quaintrell H et al *Astron. Astrophys.* **401** 313 (2003)
- [49] van Kerkwijk M H et al *Astron. Astrophys.* **303** 483 (1995)
- [50] Rappaport S *IAU Circ.* **2869** 2 (1975)
- [51] Bochkarev N G, Karitskaja E A, Shakura N I *Sov. Astron. Lett.* **1** 237 (1975)
- [52] Nagase F et al *Publ. Astron. Soc. Jap.* **38** 547 (1986)
- [53] Watanabe S et al *Astrophys. J.* **651** 421 (2006)
- [54] Staubert R *Chin. J. Astron. Astrophys. Suppl.* **3** 270 (2003)
- [55] Doroshenko V *PhD Thesis University of Tuebingen (IAAT)* (2011)
- [56] Davidsen A, Malina R, Bowyer S *Astrophys. J.* **211** 866 (1977)
- [57] Hinkle K H, Fekel F C, Joyce R R, Wood P R, Smith V V, Lebzelter T *Astrophys. J.* **641** 479 (2006)
- [58] Makishima K et al *Nature* **333** 746 (1988)
- [59] Dotani T et al *Publ. Astron. Soc. Jap.* **41** 472 (1989)
- [60] Hénault-Brunet V et al *Mon. Not. R. Astron. Soc.* **420** L13 (2012)
- [61] Haberl F et al *Astron. Astrophys.* **537** L1 (2012)
- [62] Popov S B, Turolla R *Mon. Not. R. Astron. Soc.* **421** L127 (2012)
- [63] Fu Lei, Li Xiang-Dong *Astrophys. J.* **757** 171 (2012)
- [64] Reig P, Torrejón J M, Blay P *Mon. Not. R. Astron. Soc.* **425** 529 (2012)
- [65] Ribó M et al. *Astron. Astrophys.* **449** 687 (2006)
- [66] Torrejón et al. *Astron. Astrophys.* **423** 301 (2004)
- [67] Masetti N et al. *Astron. Astrophys.* **423** 311 (2004)
- [68] Blay P et al. *Astron. Astrophys.* **438** 963 (2005)
- [69] Wang W *Mon. Not. R. Astron. Soc.* **398** 1428 (2009)
- [70] Raymond J C, Cox D P, Smith B W *Astrophys. J.* **204** 290 (1976)
- [71] Cowie L L, McKee C F, Ostriker J P *Astrophys. J.* **247** 908 (1981)
- [72] Tarter C B, Tucker W H, Salpeter E E *Astrophys. J.* **156** 943 (1969)
- [73] Hatchett S, Buff J, McCray R *Astrophys. J.* **206** 847 (1976)
- [74] Sunyaev R A, Shakura N I *Sov. Astron. Lett.* **3** 138 (1977)
- [75] Marykuty J et al *Mon. Not. R. Astron. Soc.* **407** 285 (2010)
- [76] Ducci L, Sidoli L, Paizis A *Mon. Not. R. Astron. Soc.* **408** 1540 (2010)
- [77] Landau L D, Lifshitz E M *Fluid Mechanics*(Pergamon Press, 1959)
- [78] Wasiutyński J *Studies in Hydrodynamics and Structure of Stars and Planets* (Oslo, 1946)

- [79] Shakura N I, Sunyaev R A *Adv. Space Res.* **8** 135 (1988)
- [80] Shakura N I, Sunyaev R A, Zilitinkevich S S *Astron. Astrophys.* **62** 179 (1978)
- [81] Parker E *Interplanetary dynamical processes* (New York: Interscience Publ., 1963)
- [82] Beskin V S *MHD Flows in Compact Astrophysical Objects: Accretion, Winds and Jets* (Berlin: Springer, 2010)